ELSEVIER

Nuclear Physics A 588 (1995) 559–596

NUCLEAR PHYSICS A

Nuclear wobbling motion and electromagnetic transitions

Yoshifumi R. Shimizu [a], Masayuki Matsuzaki [b]

[a] *Department of Physics, Kyushu University 33, Fukuoka 812, Japan*
[b] *Department of Physics, Fukuoka University of Education, Munakata, Fukuoka 811-41, Japan*

Received 20 September 1994; revised 13 December 1994

Abstract

The nuclear wobbling motion is studied from a microscopic viewpoint. It is shown that the expressions not only of the excitation energy but also of the electromagnetic-transition rate in the microscopic RPA framework can be cast into the corresponding forms of the macroscopic rotor model. Criteria to identify the rotational band associated with the wobbling motion are given. Examples of realistic calculations are investigated and some theoretical predictions are presented.

1. Introduction

The recent advent of new-generation crystal-ball detectors has been opening a great possibility to explore a new area of the high-spin physics. There are many interesting subjects which are waiting to be studied. Among them, we would like to concentrate, in this paper, upon the nuclear wobbling motion [1], which is one of the "exotic" rotational motions in the sense that the axis of rotation does not coincide with any of the inertia axes of a deformed nuclear body.

The nuclear wobbling motion has been considered by the analogy with the spinning motions of the asymmetric top (classical rigid body), where perturbations are superimposed on the main rotation around the principal axis with the largest moment of inertia. When the system is quantized, the energy spectra in the energy-versus-angular-momentum plane, which are nothing else but those of the well-known macroscopic triaxial-rotor model (Davydov model), are classified into two groups of rotational bands; i.e., the "horizontal" and "vertical" sequences corresponding asymptotically to the Regge trajectories associated with the largest and the smallest moment of inertia, respectively. In the high-spin limit [1], the physical meaning of those two sequences appears to be more transparent by introducing an elementary excitation of the "wobbling-phonon"

SSDI 0375-9474(94)00823-X

mode. The horizontal sequences parallel to the yrast line are rotational bands in which zero, one, and two, etc., wobbling phonons are excited in each intrinsic state, while the vertical sequences starting from each yrast state consist of the multiple wobbling-phonon bands. In fact, the E2 transition rates in the former ($|\Delta I| = 2$) are larger than that in the latter ($|\Delta I| = 1$) by an order of $1/I$ in the high-spin limit [1,2].

It is very interesting to ask whether such an "exotic" rotational motion is realized as a collective motion in atomic nuclei, because it directly reflects the three-dimensional nature of rotational motions. It should, however, be noticed that the concept of the three-dimensional rotation is meaningful only when the motion of the angular-momentum vector is traced in the "intrinsic" or the "body-fixed" frame, where the macroscopic rotor model is formulated. The very definition, however, of such a coordinate frame is not simple at all from the microscopic point of view in the general framework of the nuclear many-body theory [3–6].

Detailed experimental investigation is only possible in the discrete line spectroscopy so that the horizontal sequences in which only one or two wobbling phonons are excited are the most promising targets for our study. For such rotational bands near the yrast line, the small-amplitude approximation to the wobbling mode may be allowed. Then the fully microscopic formulation is possible [2,7–13] in terms of the random-phase approximation (RPA) on top of the cranked mean-field theory, and the analogy to the macroscopic rotor model becomes transparent. Thus we mainly concentrate, in this paper, on the yrast and the first excited wobbling bands and investigate the possible consequences predicted from the RPA theory [2] in realistic nuclei. In the course of the investigation it will be shown that not only the energy spectra but also the interband ($\Delta I = \pm 1$) electromagnetic transition probabilities can also be expressed in the same way as in the macroscopic rotor model in terms of the microscopically defined "effective" moments of inertia [2], which are introduced for the wobbling eigenfrequency.

The paper is organized as follows: The E2 transitions in the RPA theory is reviewed and is applied to the well-known γ-vibrational bands in Section 2. Some basic ingredients in the macroscopic rotor model, especially the expressions for the electromagnetic transition rates, are reviewed in Section 3. The microscopic formalism is presented in Section 4, and some examples of realistic calculations are shown in Section 5. Section 6 is devoted to concluding remarks. Some preliminary results of the present work have already been reported in Refs. [14–16].

2. E2 Transitions for the γ-vibrational band

The RPA theory on top of the cranked mean-field approach, which is suitable for the high-spin states, was first developed in Ref. [17] and applied to the high-spin β- and γ-vibrational bands [18,19]. The extension to the odd nuclei, with special attention to how the electromagnetic-transition rates should be calculated, has been done in Ref. [20].

The RPA treatment of the vibrational excitations [17] is based on the boson expansion theory; the lowest-order vacuum states, on which the RPA modes are excited, are described by the static mean-field theory uniformly rotating around one of the inertia axes (one-dimensional cranking states). Being combined with the $1/I$ expansion technique, the matrix element of the electromagnetic transition with multipolarity λ is expressed in the simple form

$$\mathcal{M}(\mathrm{i} \to \mathrm{f};\ \Delta I) \approx \langle \mathrm{f} \,|\, T_{\lambda\mu=\Delta I} \,|\, \mathrm{i} \rangle, \tag{2.1}$$

where $T_{\lambda\mu}$ is the transition operator and $\Delta I = I_\mathrm{f} - I_\mathrm{i}$. It should be stressed that the components of $T_{\lambda\mu}$ are defined with respect to the rotation (cranking) axis.

In the above formula only the lowest order of the power-series expansion in $1/I$ is retained. Although we are mainly interested in the high-spin limit and consider only the order of Eq. (2.1) in the following sections, it is worth mentioning that the equation is applicable at low spins if the the geometry of the angular-momentum vector is properly taken into account. A good example is the M1 transition in odd nuclei at relatively low angular momenta, as is shown in Ref. [21]. It is, however, noticed that the idea is more general and is based on the observation that the most important part of the spin-dependence, which comes from the dynamics but not from the kinematics of the angular-momentum algebra (the Clebsch–Gordan coefficients), is contained in the right-hand side of Eq. (2.1) through the spin-dependent change of cranked wave functions. In order to see that this is really the case and to show the reliability of the formula (2.1), we compare the results of the RPA calculations for the low-spin γ-vibrational band [19] in even–even nuclei with the experimental data in the remaining part of this section.

The quantities to be investigated are the E2 transitions between the ground-state band and the γ-vibrational band. Therefore, the initial and the final state in Eq. (2.1) are

$$|\mathrm{i}\rangle = X_\gamma^{(\pm)\dagger} \,|\, \omega_\mathrm{rot}\rangle, \quad |\mathrm{f}\rangle = |\, \omega_\mathrm{rot}\rangle, \tag{2.2}$$

where $|\, \omega_\mathrm{rot}\rangle$ is the yrast state with rotational frequency ω_rot obtained by the cranked mean-field approximation. $X_\gamma^{(\pm)\dagger}$ is the creation operator of the RPA eigenmode at the corresponding frequency and smoothly continues to the γ-vibrational solution at zero frequency. The superscript $(\pm)$ denotes the signature quantum number r carried by the RPA mode; for example, the $(+)$-band represents the even-spin member and the $(-)$-band the odd-spin one if the vacuum $|\, \omega_\mathrm{rot}\rangle$ has signature $(+)$ (i.e. $\alpha = 0$). There are five kinds of transitions associated with $\Delta I = 0,\ \pm 1,\ \pm 2$, and the B(E2)-values of these transitions are calculated by means of the electric (i.e. proton) part of the operators [20],

$$Q_{20} = \frac{1}{2} Q_0^{(+)} + \frac{\sqrt{3}}{2} Q_2^{(+)}, \tag{2.3a}$$

$$Q_{2\pm1} = \frac{i}{\sqrt{2}} \left(Q_1^{(-)} \pm Q_2^{(-)} \right), \tag{2.3b}$$

$$Q_{2\pm2} = -\frac{1}{\sqrt{2}} \left(\frac{\sqrt{3}}{2} Q_0^{(+)} + \frac{1}{2} Q_2^{(+)} \pm Q_1^{(+)} \right), \tag{2.3c}$$

where $Q_K^{(\pm)}$ ($K=0, 1, 2$) are the signature-coupled quadrupole operators [19] in which the z-axis is taken as the quantization axis while the rotation axis is chosen to be the x-axis.

Among the five transition amplitudes between the γ- and the ground-state band,

$$t\left[\left(Q_K^{(\pm)}\right)\right] \equiv \langle \mathrm{f} \,|\, Q_K^{(\pm)} \,|\, \mathrm{i}\rangle = \langle\, \omega_{\mathrm{rot}} \,|\left[Q_K^{(\pm)},\, X_\gamma^{(\pm)\dagger}\right]|\, \omega_{\mathrm{rot}}\rangle = \langle\left[Q_K^{(\pm)},\, X_\gamma^{(\pm)\dagger}\right]\rangle, \tag{2.4}$$

only the $K=2$ components are non-zero at $\omega_{\mathrm{rot}}=0$ from the selection rule because the ground state under consideration is axially symmetric. In the low-frequency limit, the electric part of them is of the form

$$t\left[\left(Q_K^{(\pm)}\right)^{(\mathrm{E})}\right] = \mathscr{E}_\gamma\left(\delta_{K2} + \delta_{K1}\alpha_\gamma\,\omega_{\mathrm{rot}}\right) + \mathrm{O}\left(\omega_{\mathrm{rot}}^2\right), \tag{2.5}$$

where the superscript (E) denotes the electric part of the transition operator. As it is mentioned we have to include the effect of Clebsch–Gordan coefficients at the low spin. In this case we need $\langle I_{\mathrm{i}}\ 2\ 2\ -2 \,|\, I_{\mathrm{f}}\ 0\rangle$ whose asymptotic values in the large-I limit are

$$|\langle I_i\ 2\ 2\ -2 \,|\, I_{\mathrm{f}}\ 0\rangle| \approx \begin{cases} \frac{1}{4}\sqrt{6}, & \Delta I = 0, \\ \frac{1}{2}, & \Delta I = \pm 1, \\ \frac{1}{4}, & \Delta I = \pm 2. \end{cases} \tag{2.6}$$

Combining Eqs. (2.3) and (2.6) and using Eq. (2.5), we have the expression of the $B(\mathrm{E2}) \equiv |\mathscr{M}(\mathrm{i}\to\mathrm{f})|^2$, which is valid in the low-spin limit,

$$\frac{B(\mathrm{E2})_{\gamma\to\mathrm{g}}^{\Delta I}}{\langle I_{\mathrm{i}}\ 2\ 2\ -2 \,|\, I_{\mathrm{f}}\ 0\rangle^2} = |\sqrt{2}\ \mathscr{E}_\gamma|^2\left[1 + a_\gamma\,\Delta I\omega_{\mathrm{rot}} + \mathrm{O}\left(\omega_{\mathrm{rot}}^2\right)\right]^2. \tag{2.7}$$

Using another asymptotic relation and the fact that the rotational frequency can be related to the angular momentum through the moment of inertia $\mathscr{J}$, i.e.

$$2I\Delta I \approx I_{\mathrm{f}}(I_{\mathrm{f}}+1) - I_{\mathrm{i}}(I_{\mathrm{i}}+1), \quad \hbar\,\omega_{\mathrm{rot}} \approx I/\mathscr{J}, \tag{2.8}$$

where $I \equiv \frac{1}{2}(I_{\mathrm{f}} + I_{\mathrm{i}})$, we finally find

$$\frac{\left[B(\mathrm{E2})_{\gamma\to\mathrm{g}}^{\Delta I}\right]^{1/2}}{\langle I_{\mathrm{i}}\ 2\ 2\ -2 \,|\, I_{\mathrm{f}}\ 0\rangle} \approx \mathscr{E}_{\mathrm{t}}\left\{1 + q\left[I_{\mathrm{f}}(I_{\mathrm{f}}+1) - I_{\mathrm{i}}(I_{\mathrm{i}}+1)\right]\right\}, \tag{2.9a}$$

to the first order. This is nothing else but the formula discussed as the generalized intensity relation in Ref. [22], where

$$\mathscr{E}_{\mathrm{t}} \equiv |\sqrt{2}\ \mathscr{E}_\gamma|, \quad q \equiv a_\gamma/2\hbar\mathscr{J}. \tag{2.9b}$$

It should be emphasized that the parameters $\mathscr{E}_{\mathrm{t}}$ and q are now calculated microscopically by means of the RPA theory at the finite rotational frequency.

An example of calculated electric quadrupole transition amplitudes (see Eq. (2.4)) is shown as functions of the rotational frequency in Fig. 1 for a typical well-deformed nucleus, ^{164}Er. The procedure of calculation is the same as in Refs. [19,20], except that

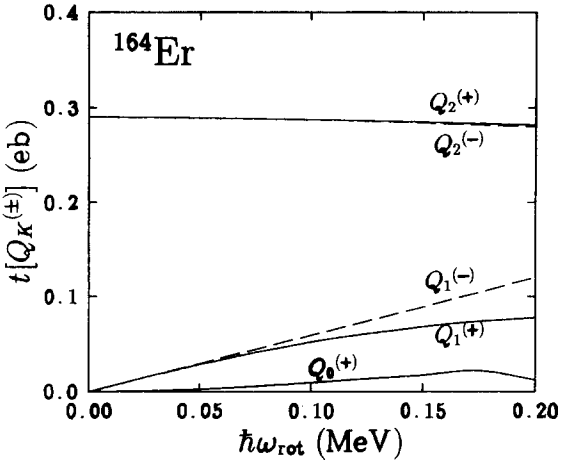

Fig. 1. The electric E2 transition amplitudes (2.4) in ^{164}Er, microscopically calculated by the RPA formalism as functions of the rotational frequency.

the difference of the oscillator frequency between neutrons and protons in the Nilsson potential and of the oscillator length in the quadrupole residual interaction [23,24] are properly treated [1]. Namely, the residual interactions of the monopole pairing and the quadrupole interactions are used, and their strengths are determined so as to reproduce the even–odd mass differences, and the excitation energies of the β-, γ-vibrations ($K = 0, 2$) and the zero-frequency (Nambu–Goldstone) mode ($K = 1$), at $\omega_{rot} = 0$, respectively. After fixing the force strengths at $\omega_{rot} = 0$, the pairing self-consistent calculations are performed as functions of the rotational frequency, but the deformation parameters are fixed at the values deduced from the experiments [25], for simplicity. When the rotational frequency increases, the quasiparticle alignments occur generally. In order to identify individual rotational bands with the same internal structure, we use the diabatic quasiparticle orbits [19], specifically the diabatic basis constructed by the method of the ω_{rot}-expansion up to the third order [20]. The model space of the Nilsson orbits with $N_{osc} = 4$–6 is chosen for neutrons and those with $N_{osc} = 3$–5 for protons. It reproduces the transition amplitudes very well without using any kind of the effective charge (see below).

It is seen from the figure that the amplitudes follow the low-frequency behaviour given by Eq. (2.5) and the parameters, $\mathscr{C}_\gamma$ and a_γ, are easily extracted. The values thus obtained for some arbitrarily chosen rare-earth nuclei are summarized in Table 1, where those of $\mathscr{C}_t$ and q in Eq. (2.9) are also listed and compared with the available experimental data. Note that the moments of inertia for the ground-state band and the

[1] In Ref. [19] the transition amplitudes of the *mass* quadrupole operators were shown for the γ-vibrational bands. For the collective RPA solutions the proper treatment of neutron and proton oscillator lengths makes the transition amplitudes of the electric operators approximately about Z/A of those of the mass operators, just as in the case of the expectation values of the quadrupole operators, i.e. the static quadrupole moments (see Eq. (4.32) and discussions at the end of Section 4).

Table 1
The first-order coefficient of the rotational-frequency-dependence calculated by the RPA theory, a_γ in Eq. (2.5), and the extracted intensity-relation parameters, $\mathscr{Q}_t$ and q in Eq. (2.9b). Here (g) and (γ) attached to the theoretical q values mean that they are obtained by Eq. (2.9b) using the experimental moment of inertia of the ground band ($\mathscr{J} \equiv \mathscr{J}_g$) and the γ-band ($\mathscr{J} \equiv \mathscr{J}_\gamma$)

Nucleus	$a_\gamma/\hbar$ [MeV^{-1}]	$\mathscr{Q}_t^{(th)}$ [$e\cdot$b]	$\mathscr{Q}_t^{(exp)}$ [$e\cdot$b]	$q^{(th)}$ (g)	$q^{(th)}$ (γ)	$q^{(exp)}$
^{162}Dy	2.0	0.37	0.35 [a]	0.027	0.024	–
^{164}Dy	1.9	0.38	0.34 [b]	0.023	0.020	0.021 [b]
^{164}Er	2.0	0.41	0.38 [c]	0.031	0.027	–
^{166}Er	1.8	0.41	0.42 [d]	0.024	0.021	0.022 [d]
^{168}Er	1.3	0.42	0.37 [e]	0.017	0.015	0.018 [e]

[a] Extracted from $B(\mathrm{E2}: 0_g^+ \to 2_\gamma^+)$ [59].
[b] Extracted from the χ^2-fitting of the matrix elements $\mathscr{M}(\mathrm{E2};\ \Delta I = 0, -2)_{\gamma\to g}$ ($I_\gamma = 2, 4, \ldots, 10$) obtained by the Coulomb-excitation experiment of Ref. [60]. There is an appreciable scattering of data from the relation, Eq. (2.9a). The weights inversely proportional to the squares of the error bars of the data are used for the χ^2-fitting.
[c] Extracted from $B(\mathrm{E2}: 0_g^+ \to 2_\gamma^+)$ [61].
[d] From Ref. [22].
[e] Extracted from the χ^2-fitting of the matrix elements $\mathscr{M}(\mathrm{E2};\ \Delta I = 0, 0, \pm 1, \pm 2)_{\gamma\to g}$ ($I_\gamma = 2, 3, \ldots, 8$) obtained by the Coulomb-excitation experiment in Ref. [62] just in the same way as note b above.

γ-vibrational band are the same in the low-spin limit within the RPA theory. This is, however, not the case in experimental data. This is because the difference of the moments of inertia results from the higher-order couplings between the vibrational and rotational motions, while these are not taken into account in the RPA. Therefore the two values of q obtained by using two choices of experimentally determined $\mathscr{J} = \mathscr{J}_g$ and $\mathscr{J} = \mathscr{J}_\gamma$ are included in the table.

The absolute values of the amplitudes are well reproduced in our calculations. However, the agreement should not be taken so seriously because the resultant transition amplitudes calculated by RPA depend on the size of the adopted model space. It is known that the calculation within the full model space usually overestimates the experimental values in the simple monopole pairing plus the quadrupole interaction model. We will not discuss this point further in this paper.

More important is that not only the sign but also the absolute values of the q-parameter are well accounted for in the present RPA theory, which is calculated from the ratio of the transition amplitudes and therefore more reliable than the amplitudes themselves. This clearly shows that the rotation-induced change of the microscopic structure of the vibrational motion, i.e. the K-mixing of the transition amplitudes (see Eq. (2.5)), is correctly described in the RPA theory. In Fig. 1 the appreciable deviations from the lowest-order relations, the order of $O(\omega_{rot}^2)$, are predicted in the region of $\hbar\omega_{rot} \gtrsim 0.15$ MeV; for example, the amount of the reduction of the $I_\gamma \to (I \pm 1)_g$ transition amplitude ($\propto t[(Q_2^{(-)} + \Delta I\, Q_1^{(-)})^{(E)}]$) is larger than that of the $I_\gamma \to (I \pm 2)_g$ transition ($\propto t[(Q_2^{(+)} + \sqrt{3}\ Q_0^{(+)} + 2\Delta I\, Q_1^{(+)})^{(E)}]$, see Eq. (2.3)). We should, however, be careful in drawing a definite conclusion from these results; at these moderate spins the other higher-order effects in $1/I$ neglected in, e.g., Eqs. (2.6) and (2.8), are of the

same order, and then all the higher-order terms should consistently be calculated. This is out of the scope of the present calculations.

3. Macroscopic rotor model

The nuclear wobbling motion was originally predicted as a collective motion in the macroscopic rotor model [1]. In order to see the characteristic features and to compare with microscopic models, the energy spectra and the E2 and M1 transition rates related to the wobbling motion in the high-spin limit are summarized in this section.

The hamiltonian of the rotor model is written in terms of the three moments of inertia around the principal axes, $\mathcal{J}_x$, $\mathcal{J}_y$ and $\mathcal{J}_z$:

$$H_{\mathrm{R}} = \frac{I_x^2}{2\mathcal{J}_x} + \frac{I_y^2}{2\mathcal{J}_y} + \frac{I_z^2}{2\mathcal{J}_z}, \tag{3.1}$$

where the angular-momentum operators are components with respect to the *body-fixed frame*. The energy eigenvalues of the above hamiltonian are well known; they are specified by two quantum numbers and are given explicitly in the large-I limit by

$$E_{\mathrm{R}}(I, n_{\mathrm{w}}) = \frac{I(I+1)}{2\mathcal{J}_x} + \hbar\omega_{\mathrm{w}}(I)\left(n_{\mathrm{w}} + \tfrac{1}{2}\right), \tag{3.2}$$

where it is assumed that $\mathcal{J}_x$ is the largest and that the main rotation occurs around the x-axis. The wobbling frequency is determined by the well-known formula [1,26]

$$\hbar\omega_{\mathrm{w}} = I\sqrt{W_y W_z} = \hbar\omega_{\mathrm{rot}}\sqrt{\frac{(\mathcal{J}_x - \mathcal{J}_y)(\mathcal{J}_x - \mathcal{J}_z)}{\mathcal{J}_y \mathcal{J}_z}}, \tag{3.3a}$$

where

$$W_y \equiv 1/\mathcal{J}_z - 1/\mathcal{J}_x, \quad W_z \equiv 1/\mathcal{J}_y - 1/\mathcal{J}_x \tag{3.3b}$$

and

$$\hbar\omega_{\mathrm{rot}} \equiv I/\mathcal{J}_x \tag{3.3c}$$

corresponds to the rotational frequency around the main rotation axis. The integer $n_{\mathrm{w}} = 0, 1, 2, \ldots$ in Eq. (3.2) is the number of wobbling phonons excited on the yrast states. Then the horizontal and vertical sequences mentioned in Section 1 are precisely given by

$$E^{(\mathrm{hor})}_{|\Delta I|=2}(I) = E_{\mathrm{R}}(I, n_{\mathrm{w}}), \quad n_{\mathrm{w}} = 0, 1, 2, \ldots, \tag{3.4a}$$

with n_{w} specifying the yrast, yrare, ... bands, and

$$E^{(\mathrm{ver})}_{|\Delta I|=1}(I) = E_{\mathrm{R}}(I, n_{\mathrm{w}} = I - K), \quad K = K_1, K_2, K_3, \ldots, \tag{3.4b}$$

with K specifying the band-head spin. Note that the number of phonons is changed in the vertical sequence but not in the horizontal one. The horizontal sequence (i.e.

$\Delta n_w = 0$) corresponds to the band connected by the E2 transitions with $\Delta I = \pm 2$ and the vertical one (i.e. $\Delta n_w = \pm 1$) to the band with $\Delta I = \pm 1$, respectively; the transition energies in these two bands are therefore given in the lowest order in $1/I$ as

$$E_\gamma^{(\mathrm{hor})} = \mp 2\hbar\omega_{\mathrm{rot}} \quad (\Delta I = \pm 2), \tag{3.5a}$$

$$E_\gamma^{(\mathrm{ver})} = \hbar\omega_w \mp \hbar\omega_{\mathrm{rot}}, \quad (\Delta I = \pm 1). \tag{3.5b}$$

The E2 transition operator in the rotor model is derived by the basic assumption that the quadrupole tensor of the rotor is diagonal in the body-fixed frame; thus

$$Q_{2\mu}^{(\mathrm{E})} = e\frac{Z}{A}R^2\left(\frac{\alpha_y + \alpha_z}{\sqrt{3}}D_{\mu,0}^{(2)} + \frac{\alpha_y - \alpha_z}{\sqrt{2}}\left(D_{\mu,2}^{(2)} + D_{\mu,-2}^{(2)}\right)\right), \tag{3.6}$$

where the quantization axis of the D-functions is the main rotation axis (x-axis), and then the transition rates are given, again within the large-I approximation, by

$$B(\mathrm{E2})_{\Delta I=\pm 2}^{(\mathrm{hor})} \approx \left(e\frac{Z}{A}\right)^2 \tfrac{1}{2}R^4(\alpha_y - \alpha_z)^2, \tag{3.7a}$$

$$B(\mathrm{E2})_{\Delta I=\pm 1}^{(\mathrm{ver})} \approx \left(e\frac{Z}{A}\right)^2 \frac{n_w}{I}R^4\left[\alpha_y\left(\frac{W_z}{W_y}\right)^{1/4} \mp \alpha_z\left(\frac{W_y}{W_z}\right)^{1/4}\right]^2, \tag{3.7b}$$

and the static Q-moment by

$$Q^{(\mathrm{E})} \approx e\frac{Z}{A}\cdot 2\sqrt{\frac{4\pi}{15}}R^2(\alpha_y + \alpha_z). \tag{3.7c}$$

Here the deformation parameters (α_y, α_z) are introduced through the static quadrupole moments as

$$\begin{aligned} R^2\alpha_y &\equiv \frac{1}{2}\sqrt{\frac{15}{4\pi}}\int(x^2 - z^2)\rho(\boldsymbol{r})\,\mathrm{d}\boldsymbol{r} = \left\langle\frac{1}{2}Q_2^{(+)} - \frac{\sqrt{3}}{2}Q_0^{(+)}\right\rangle, \\ R^2\alpha_z &\equiv \frac{1}{2}\sqrt{\frac{15}{4\pi}}\int(x^2 - y^2)\rho(\boldsymbol{r})\,\mathrm{d}\boldsymbol{r} = \langle Q_2^{(+)}\rangle. \end{aligned} \tag{3.8}$$

These parameters (α_y, α_z) can be related to the usual "(ϵ_2, γ)"-like parametrizations (ϵ_2^*, γ^*) [2] which are defined by

$$\int x_k^2\rho(\boldsymbol{r})\,\mathrm{d}\boldsymbol{r} \equiv \frac{1}{3}R^2\left[1 + \frac{4}{3}\epsilon_2^*\cos\left(\gamma^* + \frac{2\pi}{3}k\right)\right] \quad (k = 1, 2, 3 \equiv x, y, z) \tag{3.9}$$

[2] These parameters coincide with the original ones only within the first order in ϵ_2 because the original ones are defined with respect to the anisotropic harmonic-oscillator frequencies. The Lund convention for the sign of the triaxiality parameter γ is used throughout this paper.

through

$$\alpha_y = \sqrt{\frac{5}{9\pi}}\,\epsilon_2^*\,\sin\left(\gamma^* + \frac{4\pi}{3}\right), \quad \alpha_z = -\sqrt{\frac{5}{9\pi}}\,\epsilon_2^*\,\sin\gamma^*, \tag{3.10}$$

so that they represent the static triaxiality around the corresponding y-, z-axes. In the same way, $\alpha_y - \alpha_z$ is proportional to the static moment around the main rotation axis (x-axis), and then Eq. (3.7a) simply denotes the usual stretched E2 transitions. If we consider the lowest excited band, the one-phonon wobbling band, then $n_w = 1$ in Eq. (3.7b).

In the same framework, M1 transitions can be considered if an appropriate magnetic property of the rotor is assumed. Since there exist only the angular-momentum operator which has the same property as the magnetic-transition operator in the model, the most general form for the components of the magnetic-moment vector in the body-fixed frame is given by

$$m_i = \sum_{j=x,y,z} g_{ij} I_j \quad (i = x,\ y,\ z), \tag{3.11}$$

where $g_{ij} = g_{ji}$ $(i,\ j = x,\ y,\ z)$ denotes the g-factor tensor in the body-fixed frame. Then the M1 transition operator is written as

$$\mu_{1\mu} = \sqrt{\frac{3}{4\pi}}\,\mu_N \sum_{\nu\rho} g_{\nu\rho}\tfrac{1}{2}\left\{D^{(1)}_{\mu\nu},\ I_\rho\right\}, \tag{3.12}$$

where μ_N is the nuclear magneton. The B(M1)'s are evaluated in the same way as B(E2). It should be noted that the presence of the non-diagonal terms of the g-factor tensor causes the horizontal transitions (i.e. $\Delta n_w = 0$) with $\Delta I = \pm 1$ and the vertical ones (i.e. $\Delta n_w = \pm 1$) with $\Delta I = 0$ as well as the $\Delta I = \pm 1$ vertical transitions. The results are given again in the lowest order in $1/I$ as [3]

$$B(\mathrm{M1})^{(\mathrm{hor})}_{\Delta I=\pm 1} \approx \frac{3}{4\pi}\mu_N^2 \frac{I^2}{2}\left(g_{xy}^2 + g_{xz}^2\right), \tag{3.13a}$$

$$B(\mathrm{M1})^{(\mathrm{ver})}_{\Delta I=0} \approx \frac{3}{4\pi}\mu_N^2 n_w (2I)\left(g_{xy}^2\sqrt{\frac{W_y}{W_z}} + g_{xz}^2\sqrt{\frac{W_z}{W_y}}\right), \tag{3.13b}$$

$$B(\mathrm{M1})^{(\mathrm{ver})}_{\Delta I=\pm 1} \approx \frac{3}{4\pi}\mu_N^2 n_w \frac{I}{4}\left\{\left[(g_{yy} - g_{xx})\left(\frac{W_y}{W_z}\right)^{1/4} \mp (g_{zz} - g_{xx})\left(\frac{W_z}{W_y}\right)^{1/4}\right]^2 + g_{yz}^2\left[\left(\frac{W_y}{W_z}\right)^{1/4} \pm \left(\frac{W_z}{W_y}\right)^{1/4}\right]^2\right\}, \tag{3.13c}$$

[3] The M1 transitions in the rotor model have been studied in Ref. [27], in which the magnetic-moment vector is assumed to be of the same form as in Eq. (3.11) but with only diagonal components, $g_{ij} = g_i\delta_{ij}$. Their M1 operator is, however, different from that given in Eq. (3.12), which seems incorrect. Consequently the resultant B(M1) is also different from that given in Eq. (3.13c) even with $g_{ij} = g_i\delta_{ij}$.

and the g-factor of the system by

$$g_R \approx g_{xx}. \tag{3.13d}$$

Note that $g_{xy} = g_{xz} = 0$ if the signature symmetry (under the π-rotation around the x-axis) is imposed in the body-fixed frame. Then both the $\Delta I = \pm 1$ horizontal transition (3.13a) and the $\Delta I = 0$ vertical transition (3.13b) naturally vanish.

It should be noted that the I-dependence of the observables is generally different; for example, $B(\mathrm{E2})^{(\mathrm{ver})}_{\Delta I=\pm 1} \propto 1/I$ and $B(\mathrm{M1})^{(\mathrm{ver})}_{\Delta I=\pm 1} \propto I$, while $B(\mathrm{E2})^{(\mathrm{hor})}_{\Delta I=\pm 2}$ does not depend on I (up to the leading order in $1/I$), if all the parameters, i.e. the quadrupole deformations, α_y and α_z, the moments of inertia, $\mathcal{J}_x$, $\mathcal{J}_y$ and $\mathcal{J}_z$, and the g-factor tensor, g_{ij}, are constant against I. Actually, all these parameters are not independent of each other; for example, the quadrupole deformations determine the moments of inertia in the original rigid-body model. However, if one wants to apply the model to realistic nuclei, one should consider that all the parameters depend smoothly on the angular momentum, and the moments of inertia do not necessarily take the rigid-body values. As will be discussed in the following sections, the microscopically calculated $\mathcal{J}_x$, $\mathcal{J}_y$ and $\mathcal{J}_z$ change as functions of the rotational frequency and the relationships between them are far from those of the rigid body [28].

It is worth mentioning that the axially symmetric limit should be taken with great care. There are two kind of limits: The "collective-rotation" limits, where $\gamma = 0°$, $-60°$, or equivalently either $\alpha_z = 0$ or $\alpha_y = 0$, and the "non-collective-rotation" limits where $\gamma = 60°$, $-120°$, or $\alpha_y = \alpha_z$. In the former limits, it is easy to see that there are no definite limiting expressions for the wobbling energy and the $\Delta I = \pm 1$ $B(\mathrm{E2})$ and $B(\mathrm{M1})$, as long as the detailed limiting behaviours of the three moments of inertia are not specified. In contrast, one can always argue the latter limits, where $\mathcal{J}_y = \mathcal{J}_z$ so that $W_y = W_z$. From Eq. (3.7), the $\Delta I = +1$ vertical transition as well as the $\Delta I = \pm 2$ horizontal transitions are prohibited. In fact, in this axially symmetric limit of the "non-collective rotation", the horizontal rotational sequences disappear and only the band heads with $\langle I_x \rangle = K$ are physically meaningful as the vacuum states (not the vacuum band). The collective rotation in this case, therefore, is the rotation perpendicular to the symmetry axis which is at the same time the non-collective-rotation axis (x-axis). The band consists of multiple wobbling phonons with excitation energy

$$E^{(\mathrm{ver})}_{\gamma}(K) = \hbar\omega_{\mathrm{w}}(K) + \hbar\omega_{\mathrm{rot}} \approx K/\mathcal{J}_{\perp} \quad (\mathcal{J}_{\perp} \equiv \mathcal{J}_y = \mathcal{J}_z), \tag{3.14}$$

where Eqs. (3.5b) and (3.3) are used, and with the transfer angular momentum $\Delta I = +1$ excited on the high-K band-head (vacuum) states; namely,

$$E^{(\mathrm{ver})}_{|\Delta I|=1}(I) \approx \left[I(I+1) - K^2\right]/2\mathcal{J}_{\perp} + \mathrm{const.} \quad (I \gtrsim K), \tag{3.15}$$

consistent with the large $I \approx K$ approximation. Note that the rotational frequency $\hbar\omega_{\mathrm{rot}} = K/\mathcal{J}_x$ disappears in the final expressions as it should be, because it is not the collective rotational frequency in this case. This kind of rotational band is specifically called a "precession band" and is often observed as a band excited on top of a high-K isomer state. It has been well studied microscopically both in realistic nuclei [29,30] and in a schematic model [31].

From the microscopic viewpoint, there is a collective motion even in the limit of axial symmetry of the "collective" rotation, $\gamma = 0°$ and $-60°$; this is nothing else but the γ-vibration with signature $\alpha = 1$ which has just been considered in the previous section. The reason why the limit does not behave well is that the "body-fixed" frame or the "principal-axis" frame (see the next section) of the quadrupole tensor is not well-defined in this limit. The calculation in the previous section corresponds to the one in the "uniformly rotating" frame, which is always possible to define. It will explicitly be shown in the next section that the transformation to the "principal-axis" frame is impossible in the "collective-rotation" limit from the microscopic viewpoint.

4. Microscopic RPA treatment

Although the wobbling motion is a kind of oscillatory motion of the rotation axis, the shape degrees of freedom are necessary to consider. Especially important are the non-diagonal parts of the quadrupole tensor, and thus we introduce

$$\begin{aligned} Q_y &\equiv Q_1^{(-)} = -\frac{1}{2}\sqrt{\frac{15}{4\pi}} \sum_{a=1}^{A} (xz)_a, \\ Q_z &\equiv Q_2^{(-)} = i\frac{1}{2}\sqrt{\frac{15}{4\pi}} \sum_{a=1}^{A} (xy)_a, \end{aligned} \tag{4.1}$$

which just appear as the $\Delta I = \pm 1$ E2 transition operators in Eq. (2.3b). One should note that only the modes with signature $(-)$ $(\alpha = 1)$ are relevant in the RPA order so that only these modes are considered in the following. In higher order, however, one should also consider the remaining non-diagonal component [4,5], $Q_x \equiv Q_1^{(+)}$, and the RPA eigenmodes with signature $(+)$ $(\alpha = 0)$.

In the RPA treatment, the in-band $\Delta I = \pm 2$ E2 transition does not change the number of phonons, and then the matrix elements in the vacuum (or yrast) band and the one-phonon wobbling band are the same. In contrast, the interband transition from the one-phonon wobbling to the vacuum band reflects the nature of the wobbling motion itself. From the discussions in Section 2 (see Eqs. (2.1) and (2.3c)) we have

$$B(\mathrm{E2})^{(\text{in-band})}_{\Delta I=\pm 2} \approx \langle Q^{(\mathrm{E})}_{2\pm 2}\rangle^2 = \left(e\frac{Z}{A}\right)^2 \tfrac{1}{2}R^4(\alpha_y - \alpha_z)^2, \tag{4.2a}$$

where we have used Eq. (3.8) with an understanding that the deformation parameters are those associated with the vacuum states $|\,\omega_{\mathrm{rot}}\rangle$, and

$$B(\mathrm{E2})^{(\text{inter})}_{n,\Delta I=\pm 1} \approx \tfrac{1}{2}\left\{\left[\mathscr{Q}_y(n) \mp \mathscr{Q}_z(n)\right]^{(\mathrm{E})}\right\}^2, \tag{4.2b}$$

where n means that the nth RPA eigenmode is considered and the RPA transition amplitudes are defined as

$$\mathscr{Q}_k(n) \equiv \langle n\,|\,Q_k\,|0\rangle_{\mathrm{RPA}} = \langle [X_n, Q_k]\rangle \quad (k = y, z), \tag{4.3}$$

with X_n being the annihilation operator of the nth RPA eigenmode. Note that Q_z is anti-hermitian while Q_y is hermitian, and this is the reason why the sign in Eq. (4.2b) is changed from that in Eq. (2.3b). Here and hereafter, $\langle O \rangle$ for any operator O denotes the expectation value with respect to the cranked state $|\, \omega_{\rm rot} \rangle$. It is clear that the expression of the in-band E2 transition formally coincides with those of the horizontal transition in the macroscopic rotor model in Eq. (3.7a). How about the interband transition? It is one of the main purposes of this section to clarify this point.

The part of the operators Q_y and Q_z, relevant in the RPA order, can be expanded in terms of the RPA eigenmodes,

$$\begin{aligned} (Q_y)_{\rm RPA} &= \sum_{n:\rm all} \left[\mathscr{Q}_y(n) X_n^\dagger + \text{h.c.} \right], \\ (Q_z)_{\rm RPA} &= \sum_{n:\rm all} \left[\mathscr{Q}_z(n) X_n^\dagger - \text{h.c.} \right]. \end{aligned} \tag{4.4}$$

Here (n:all) means that the contribution of the Nambu–Goldstone (NG) mode,

$$X_{\rm NG}^\dagger = \frac{1}{\sqrt{2I}} (J_z + iJ_y)_{\rm RPA}, \quad I \equiv \langle J_x \rangle, \tag{4.5}$$

should be included:

$$\begin{aligned} \mathscr{Q}_y(n = \text{NG}) &= -\frac{1}{\sqrt{2I}} 2R^2 \alpha_y, \\ \mathscr{Q}_z(n = \text{NG}) &= \frac{1}{\sqrt{2I}} 2R^2 \alpha_z. \end{aligned} \tag{4.6}$$

Namely, the contribution of the NG mode corresponds to the "static" deformation while those of the normal mode to the "dynamic" (or vibrational) deformations. It should be mentioned that there exists a kind of "sum rule" [4] which relates both contributions:

$$\sum_{n \neq \rm NG} \mathscr{Q}_y(n) \mathscr{Q}_z(n) = \frac{R^4}{I} 2\alpha_y \alpha_z. \tag{4.7}$$

This sum-rule relation can be easily verified from the identity

$$[Q_y, Q_z] = 0. \tag{4.8}$$

4.1. Wobbling motion in the PA frame

Although it is not stated explicitly, up to now we have been working in the so-called "uniformly rotating" (UR) frame in the sense that all observables are based on the vacuum state $|\, \omega_{\rm rot} \rangle$ which is the cranked state rotating uniformly around one of the

[4] Strictly speaking, it cannot be called a sum rule because each term in the summation in Eq. (4.7) is not positive definite.

principal axes of the deformation of the mean field. In the macroscopic rotor model the shape is fixed but the orientation of the rotation axis is allowed to vibrate, while the rotation axis is fixed and the shape is allowed to vibrate in the RPA formalism in the UR-frame picture. In order to interpret the vibrational mode in the UR frame as the wobbling motion, we must introduce the body-fixed frame, or the "principal-axis" (PA) frame [2].

It is not trivial to define the PA frame in the general framework of the many-body problem. One must introduce "gauge conditions" [3,6] which are common in the quantum theory with constraints. According to Refs. [2,4], we impose the condition that the non-diagonal part of the quadrupole tensor should vanish:

$$(Q_k)_{\mathrm{PA}} = 0 \quad (k = x,\ y,\ z). \tag{4.9}$$

The meaning of these conditions are apparent. The PA- and UR-frame pictures are related through the Euler angles which are now the dynamical variables; for example,

$$(J_i)_{\mathrm{UR}} = \sum_{k=x,y,z} D_{ik}(\Theta)(J_k)_{\mathrm{PA}}, \tag{4.10a}$$

$$(Q_{ij})_{\mathrm{UR}} = \sum_{k,l=x,y,z} D_{ik}(\Theta) D_{jl}(\Theta)(Q_{kl})_{\mathrm{PA}}, \tag{4.10b}$$

where Q_{ij} is the non-spherically coupled representation of the quadrupole tensor, $Q_k = Q_{ij}$ (ijk:cyclic) and $D_{ij}(\Theta)$ is the D-function of rank 1 with Euler angles Θ. The three conditions, Eq. (4.9), in principle, define the microscopic structure of the three Euler angles in terms of the complete set of the observables in the UR frame, where every microscopic quantity is well-defined, and remove the redundancy between the microscopic variables in the PA frame and the collective variables Θ. Of course the situation is not so simple; for instance, what is the correct ordering between the Euler-angle operators and the microscopic quadrupole tensor in Eq. (4.10b)? One must work very carefully in a consistent framework [3].

Fortunately, it has been shown that the small-amplitude approximation makes the situation quite simple [2,6]. The Euler angles can be written in terms of the microscopic variables and then the transformation from the UR to the PA frame can be done explicitly by using them within the RPA order [2]; for example,

$$\begin{aligned}
(J_x)_{\mathrm{PA}} &= (J_x)_{\mathrm{UR}}, \\
(iJ_y)_{\mathrm{PA}} &= \left(iJ_y - \frac{I}{2R^2\alpha_z} Q_z \right)_{\mathrm{UR}}, \\
(J_z)_{\mathrm{PA}} &= \left(J_z + \frac{I}{2R^2\alpha_y} Q_y \right)_{\mathrm{UR}},
\end{aligned} \tag{4.11}$$

or the Q-operators related to the E2 transitions can be expressed by

$$\begin{aligned}
(Q_y)_{\mathrm{UR}} &= -\frac{2R^2\alpha_y}{I}\left[(J_z)_{\mathrm{UR}} - (J_z)_{\mathrm{PA}}\right], \\
(Q_z)_{\mathrm{UR}} &= \frac{2R^2\alpha_z}{I}\left[(iJ_y)_{\mathrm{UR}} - (iJ_y)_{\mathrm{PA}}\right].
\end{aligned} \tag{4.12}$$

By using the UR-frame relations (4.4) the angular-momentum operators in the PA frame are written in terms of the microscopic RPA eigenmodes,

$$\begin{aligned}(iJ_y)_{\mathrm{PA}} &= -I \sum_{n\neq \mathrm{NG}} \left(\frac{\mathscr{Q}_z(n)}{2R^2\alpha_z} X_n^\dagger - \mathrm{h.c.} \right), \\ (J_z)_{\mathrm{PA}} &= I \sum_{n\neq \mathrm{NG}} \left(\frac{\mathscr{Q}_y(n)}{2R^2\alpha_y} X_n^\dagger + \mathrm{h.c.} \right).\end{aligned} \tag{4.13}$$

Namely, the NG-mode contribution disappears. Apparently the transformation from the UR to the PA frame is possible only in the case where $\alpha_y \neq 0$ and $\alpha_z \neq 0$ (see Eq. (4.21) below for more strict conditions). Now it is easy to check, with the help of the sum-rule relation (4.7), that one of the commutation relations in the PA frame, the sign of which is opposite to the one in the UR frame, holds again within the RPA order [2],

$$\left[(iJ_y)_{\mathrm{PA}}, (J_z)_{\mathrm{PA}} \right]_{\mathrm{RPA}} = +I = \langle (J_x)_{\mathrm{PA}} \rangle. \tag{4.14}$$

It should be noticed that the transformation from the laboratory frame to the UR frame is unitary while that from the UR to PA is not, as is clear from this commutation relation. The physical reason why the transformation from UR to PA is non-unitary is apparent; the Euler angles in Eq. (4.10) are not simple parameters but are now considered to be the dynamical variables corresponding canonically to the collective angular momenta. This is a common feature for the theory with constraints [3,6].

Next, let us consider the dynamics in the PA frame. The time-dependence in the UR frame is governed by the hamiltonian

$$H_{\mathrm{UR}} \equiv H - \omega_{\mathrm{rot}} J_x. \tag{4.15}$$

Since the Euler angles are the dynamical variables describing the wobbling of the rotation axis, the hamiltonian in the PA frame is modified,

$$\begin{aligned}H_{\mathrm{PA}} &= H - \Omega_x J_x - \Omega_y J_y - \Omega_z J_z \\ &\approx H_{\mathrm{UR}} - \Omega_y J_y - \Omega_z J_z,\end{aligned} \tag{4.16}$$

where the operators on the right-hand side are in the UR frame. We omit $()_{\mathrm{UR}}$ hereafter. The quantities Ω_k $(k = x, y, z)$ in Eq. (4.16) are angular-frequency operators, which are related to the time derivatives of the Euler angles, and within the RPA order

$$\Omega_x \approx \omega_{\mathrm{rot}} \gg \Omega_y, \Omega_z,$$

reflecting the small-amplitude RPA ansatz. The microscopic structure of the angular-frequency operators are determined by the consistency conditions of the gauge conditions [2,6],

$$i\frac{\mathrm{d}}{\mathrm{d}t}(Q_k)_{\mathrm{PA}} \equiv ([Q_k, H_{\mathrm{PA}}])_{\mathrm{PA}} = 0 \quad (k = x, y, z). \tag{4.17}$$

Again within the RPA order, we obtain

$$
\begin{aligned}
i\Omega_y &= -\frac{1}{2\hbar R^2\alpha_y}\left(\left[H_{\mathrm{UR}}, Q_y\right]\right)_{\mathrm{PA}} \\
&= -\sum_{n\neq \mathrm{NG}}\left[\left(\omega_n\frac{\mathscr{Q}_y(n)}{2R^2\alpha_y}+\omega_{\mathrm{rot}}\frac{\mathscr{Q}_z(n)}{2R^2\alpha_z}\right)X_n^{\dagger}-\mathrm{h.c.}\right], \qquad (4.18)\\
\Omega_z &= \frac{1}{2\hbar R^2\alpha_z}\left(\left[H_{\mathrm{UR}}, Q_z\right]\right)_{\mathrm{PA}} = \sum_{n\neq \mathrm{NG}}\left[\left(\omega_n\frac{\mathscr{Q}_z(n)}{2R^2\alpha_z}+\omega_{\mathrm{rot}}\frac{\mathscr{Q}_y(n)}{2R^2\alpha_y}\right)X_n^{\dagger}+\mathrm{h.c.}\right],
\end{aligned}
$$

where the following results of the RPA eigenvalue problem in the UR frame are used in the second equality in each equation:

$$
H_{\mathrm{UR}} \approx \sum_{n:\mathrm{all}}\hbar\omega_n X_n^{\dagger}X_n = \sum_{n\neq \mathrm{NG}}\hbar\omega_n X_n^{\dagger}X_n + \frac{\hbar\omega_{\mathrm{rot}}}{2I}\left[\left(J_z\right)^2_{\mathrm{RPA}} - \left(iJ_y\right)^2_{\mathrm{RPA}}\right]. \qquad (4.19)
$$

Eqs. (4.13) and (4.18) show that both the angular-momentum vector and the angular-frequency vector precess around the main rotation axis (x-axis) in the PA frame with the amplitudes

$$
\left(J_k\right)_{\mathrm{PA}}(n) \equiv \langle n|\left(J_k\right)_{\mathrm{PA}}|0\rangle_{\mathrm{RPA}}, \quad \Omega_k(n) \equiv \langle n|\,\Omega_k\,|0\rangle_{\mathrm{RPA}} \quad (k=y,\ z). \qquad (4.20)
$$

For this picture to be consistent, the ratios of the dynamic deformation to the static one should be small, i.e.,

$$
\begin{aligned}
r_y(n) &\equiv \frac{\mathscr{Q}_y(n)}{2R^2\alpha_y} = \frac{\left(J_z\right)_{\mathrm{PA}}(n)}{I} \sim \mathrm{O}\left(\frac{1}{\sqrt{I}}\right) \ll 1,\\
r_z(n) &\equiv \frac{\mathscr{Q}_z(n)}{2R^2\alpha_z} = -\frac{\left(iJ_y\right)_{\mathrm{PA}}(n)}{I} \sim \mathrm{O}\left(\frac{1}{\sqrt{I}}\right) \ll 1.
\end{aligned} \qquad (4.21)
$$

The "effective" moments of inertia for each RPA eigenmode[2], which are naturally introduced through

$$
\hbar\mathscr{I}_k^{\mathrm{eff}}(n) \equiv \left(J_k\right)_{\mathrm{PA}}(n)/\Omega_k(n) \quad (k=y,\ z), \qquad (4.22)
$$

are thus written as

$$
\begin{aligned}
\hbar\mathscr{I}_y^{\mathrm{eff}}(n) &= \frac{Ir_z(n)}{\omega_n r_y(n)+\omega_{\mathrm{rot}}r_z(n)},\\
\hbar\mathscr{I}_z^{\mathrm{eff}}(n) &= \frac{Ir_y(n)}{\omega_n r_z(n)+\omega_{\mathrm{rot}}r_y(n)},
\end{aligned} \qquad (4.23)
$$

where Eqs. (4.13) and (4.18) and the definition (4.21) are used. Introducing the quantities (cf. Eq. (3.3b))

$$\begin{aligned} W_y(n) &\equiv 1/\mathcal{J}_z^{\rm eff}(n) - 1/\mathcal{J}_x \\ W_z(n) &\equiv 1/\mathcal{J}_y^{\rm eff}(n) - 1/\mathcal{J}_x \end{aligned} \quad (\mathcal{J}_x \equiv I/\hbar\omega_{\rm rot}), \tag{4.24}$$

we have

$$\begin{cases} \hbar\omega_n r_y(n)/r_z(n) = IW_z(n), \\ \hbar\omega_n r_z(n)/r_y(n) = IW_y(n), \end{cases} \tag{4.25}$$

from which the well-known wobbling energy formula is obtained in the same way as Eq. (3.3a),

$$\hbar\omega_n = I\sqrt{W_y(n)W_z(n)} = \hbar\omega_{\rm rot}\sqrt{\frac{\left[\mathcal{J}_x - \mathcal{J}_y^{\rm eff}(n)\right]\left[\mathcal{J}_x - \mathcal{J}_z^{\rm eff}(n)\right]}{\mathcal{J}_y^{\rm eff}(n)\,\mathcal{J}_z^{\rm eff}(n)}}\,. \tag{4.26}$$

This result has been first obtained in Ref. [2]. Note that the right-hand side of this equation depends on the eigenmode itself so that it is only a formal solution of the RPA equation, to which Eq. (4.25) is equivalent. It may be worth noticing that the eigenvalue equation (4.25) can be obtained by the Euler equation for the PA angular-momentum vector, which can be derived from the TDHF variational principle [2,4]. In fact, the Euler equation with the PA hamiltonian (4.16),

$$\frac{\rm d}{{\rm d}t}(J_i)_{\rm PA} = \sum_{jk}\varepsilon_{ijk}(J_j)_{\rm PA}\,\Omega_k, \tag{4.27}$$

leads to, for the component of the nth RPA eigenmode,

$$\begin{cases} -\omega_n(iJ_y)_{\rm PA}(n) = \Omega_z(n)I - \omega_{\rm rot}(J_z)_{\rm PA}(n), \\ -\omega_n(J_z)_{\rm PA}(n) = i\Omega_y(n)I - \omega_{\rm rot}(iJ_y)_{\rm PA}(n), \end{cases} \tag{4.28}$$

which reduces to Eq. (4.25) by substituting $\Omega_{y,z}(n) = (J_{y,z})_{\rm PA}(n)/\hbar\mathcal{J}_{y,z}^{\rm eff}(n)$ (Eq. (4.22)) first and $(iJ_y)_{\rm PA}(n) = -Ir_z(n)$ and $(J_z)_{\rm PA}(n) = Ir_y(n)$ (Eq. (4.21)) next.

In Refs. [12,13] the wobbling motion is studied by using the BRST formalism. We found that the microscopic angle operators, θ_y and θ_z, used for the gauge fixing in their formalism can be related to the RPA phonon operator by

$$\theta_y = \sqrt{\frac{\Delta_y}{2I\Delta_z}}\left(X_n^\dagger + X_n\right) - \frac{1}{I}(J_z)_{\rm RPA},$$

$$\theta_z = -i\sqrt{\frac{\Delta_z}{2I\Delta_y}}\left(X_n^\dagger - X_n\right) + \frac{1}{I}(J_y)_{\rm RPA},$$

once the nth normal mode is chosen. Here $\Delta_y^2 = 1/\mathcal{J}_y - 1/\mathcal{J}_x$, $\Delta_z^2 = 1/\mathcal{J}_z - 1/\mathcal{J}_x$, and so the relation contains the "y- and z-moments of inertia", $\mathcal{J}_{y,z}$. It should, however, be noticed that these two moments of inertia *cannot* be determined separately by the basic

equation for θ_y and θ_z, which is equivalent to the RPA equation in the UR frame, but only a combination of them has a definite value, i.e. $I\Delta_y\Delta_z = \hbar\omega_n$; namely, they are not physical quantities [5]. Their expressions [13] for the multipole transition operators also contain these $\mathcal{J}_{y,z}$. In spite of their appearance, we found that these unphysical quantities completely cancel out and their formulas completely coincide with those given in Ref. [17] within the RPA order, i.e., Eq. (2.1). This result makes sense: The choice of the normal mode n and the quantities $\mathcal{J}_{y,z}$ corresponds to a kind of gauge fixing so that they should not appear in the final expression of physical observables [32].

4.2. Electromagnetic transitions

Since we are considering the case where eigenvalues of all RPA solutions are real and positive, the signs of $W_y(n)$ and $W_z(n)$ are the same and then the basic equation (4.25) can be formally solved for the quantities $r_y(n)$ and $r_x(n)$:

$$\begin{aligned} r_y(n) &= c_n \frac{1}{\sqrt{2I}} \left(\frac{W_z(n)}{W_y(n)} \right)^{1/4}, \\ r_z(n) &= \sigma_n c_n \frac{1}{\sqrt{2I}} \left(\frac{W_y(n)}{W_z(n)} \right)^{1/4}, \end{aligned} \tag{4.29}$$

where σ_n denotes the sign of $W_y(n)$ (= the sign of $W_z(n)$) and the quantity c_n is the amplitude with which the nth mode contributes to the sum rule (4.7),

$$\sum_{n\neq \mathrm{NG}} r_y(n) r_z(n) = \frac{1}{2I} \Leftrightarrow \sum_{n\neq \mathrm{NG}} \sigma_n c_n^2 = 1, \tag{4.30}$$

so that $c_n^2 \ll 1$ for non-collective solutions and $c_n^2 \approx 1$ for collective solutions. Using the definition of $r_y(n)$ and $r_z(n)$ (Eq. (4.21)), the result (4.29) shows that the transition amplitudes $\mathcal{Q}_y(n)$ and $\mathcal{Q}_z(n)$ can be expressed in terms of the static-deformation parameters and the effective moments of inertia. Inserting them into Eq. (4.2b), we finally obtain

$$B(\mathrm{E2})^{(\mathrm{inter})}_{n,\Delta I=\pm 1} \approx \left(e\frac{Z}{A} \right)^2 \frac{1}{I} R^4 c_n^2 \left[\alpha_y \left(\frac{W_z(n)}{W_y(n)} \right)^{1/4} \mp \sigma_n \alpha_z \left(\frac{W_y(n)}{W_z(n)} \right)^{1/4} \right]^2, \tag{4.31}$$

where we have assumed that

$$\mathcal{Q}_k^{(\mathrm{E})}(n) \approx e\frac{Z}{A}\mathcal{Q}_k(n) \quad (k = y,\ z), \tag{4.32}$$

[5] Although their $\mathcal{J}_{y,z}$ are different form our $\mathcal{J}^{\mathrm{eff}}_{y,z}$, Δ_y^2 and Δ_z^2 correspond to our $W_z(n)$ and $W_y(n)$ in Eq. (4.24), respectively. In our formalism the requirement (4.22) completely determines $\mathcal{J}^{\mathrm{eff}}_{y,z}$.

which is approximately satisfied for the (isoscalar) collective RPA solutions. Now the analogy with Eq. (3.7b) (with $n_w = 1$) in the macroscopic rotor model is clear; the main difference, except for the assumption (4.32), is that there are many solutions, the amplitude c_n^2 is not necessarily equal to one, and the sign σ_n can be negative in the microscopic RPA treatment. Note that the negative sign $\sigma_n = -1$ means $\mathcal{J}_{y,z}^{\rm eff}(n) > \mathcal{J}_x$ or $\mathcal{J}_{y,z}^{\rm eff}(n) < 0$. This conflicts with our basic assumptions that the x-axis is the main rotation axis and the introduced three moments of inertia are physically meaningful. The interpretation of the nth RPA mode as a wobbling motion is not justified in such a case. Thereby we use the conditions $\sigma_n > 0$ (i.e. $r_y(n) r_z(n) > 0$) and $c_n^2 \approx 1$ as criteria to identify the wobbling solutions among the microscopic RPA eigenmodes in later applications.

The microscopic expression for the M1 transition rates are given[17] by Eq. (2.1) using the M1 operator as $T_{\lambda\mu}$:

$$B(\mathrm{M1})_{n,\Delta I=0}^{(\mathrm{inter})} \approx \left[\, \mu_x(n)\right]^2 = 0, \tag{4.33a}$$

$$B(\mathrm{M1})_{n,\Delta I=\pm 1}^{(\mathrm{inter})} \approx \tfrac{1}{2}\left[i\mu_y(n) \pm \mu_z(n)\right]^2, \tag{4.33b}$$

with

$$\mu_i = \sqrt{\frac{3}{4\pi}}\, \mu_{\rm N}(g_l l_i + g_s s_i), \quad \mu_i(n) \equiv \langle n|\, \mu_i\, |0\rangle_{\rm RPA} \quad (i = x,\ y,\ z), \tag{4.34}$$

where g_l and g_s are usual orbital and spin g-factors. Here we are mainly concerned with the even–even nuclei so that only the vibrational contributions are included [20]. The $\Delta I = 0$ interband transition (4.33a) vanishes identically because μ_x is the operator with signature $(+)$ $(\alpha = 0)$ while the wobbling mode belongs to the signature $(-)$ sector.

For the E2 transitions we have used the same basic requirement as the one in the macroscopic model such that the quadrupole tensor is diagonal in the PA frame, and obtained the results in the RPA corresponding to those in the rotor model. It should, however, be stressed that we cannot expect a similar correspondence for the M1 transitions. This is because the basic assumption of the M1 operator in the rotor model, Eq. (3.11) or (3.12), is not always justified from the microscopic viewpoint; for instance, the effects of quasineutron or quasiproton alignments on the M1 transitions, which are shown to be very important in the following sections, cannot be taken into account. Moreover, it is not straightforward to estimate the g-factor tensor in Eq. (3.11), in contrast to the case of E2 transitions where the static deformations in Eq. (3.8) can be microscopically calculated.

Nevertheless, it is interesting to see what is obtained if we take the same assumption as the rotor model for the M1 transition operator, namely,

$$\mu_i = \sqrt{\frac{3}{4\pi}}\, \mu_{\rm N} \sum_{j=x,y,z} (g_{ij} - g_{xx}\delta_{ij})(J_j)_{\rm PA} \quad (i = x,\ y,\ z), \tag{4.35}$$

where the fact is used that only the perpendicular component of the magnetic-moment vector to the angular momentum in the PA frame, i.e. $\boldsymbol{m} - g_{xx}\boldsymbol{I}$ in the lowest order in $1/I$, can contribute to the transition. The matrix element of $(J_x)_{\mathrm{PA}}$ vanishes like in Eq. (4.33a), and then by using Eqs. (4.11), (4.21) and (4.29), we can easily obtain

$$B(\mathrm{M1})^{(\mathrm{inter})}_{n,\Delta I=0} \approx \frac{3}{4\pi}\mu_{\mathrm{N}}^2 \frac{I}{2} c_n^2 \left(g_{xy}^2 \sqrt{\frac{W_y(n)}{W_z(n)}} + g_{xz}^2 \sqrt{\frac{W_z(n)}{W_y(n)}} \right), \tag{4.36}$$

$$\begin{aligned} B(\mathrm{M1})^{(\mathrm{inter})}_{n,\Delta I=\pm 1} \approx \frac{3}{4\pi}\mu_{\mathrm{N}}^2 \frac{I}{4} c_n^2 \Bigg\{ & \left[(g_{yy} - g_{xx}) \left(\frac{W_y(n)}{W_z(n)} \right)^{1/4} \right. \\ & \left. \mp \sigma_n (g_{zz} - g_{xx}) \left(\frac{W_z(n)}{W_y(n)} \right)^{1/4} \right]^2 \\ & + g_{yz}^2 \left[\left(\frac{W_y(n)}{W_z(n)} \right)^{1/4} \pm \sigma_n \left(\frac{W_z(n)}{W_y(n)} \right)^{1/4} \right]^2 \Bigg\}, \end{aligned} \tag{4.37}$$

which are similar expressions to those in the rotor model, Eqs. (3.13b) and (3.13c), respectively [6]. The $\Delta I = 0$ interband transition (4.36) vanishes if the signature symmetry is imposed, because then $g_{xy} = g_{xz} = 0$, just as in the case of the rotor model. This is consistent with the RPA result (4.33a) where the signature symmetry is assumed.

4.3. Collectivities of RPA solutions

In the following let us discuss general features of the high-spin RPA eigenmodes. The properties of the solutions can be different from case to case depending on the microscopic structure of vacuum states. Until now, we have used the term "collective" somewhat ambiguously. We should make it more precise here. The collectivity is usually referred to in, at least, two different contexts: (1) the transition matrix elements of observables characteristic to the solutions are large, and (2) the RPA amplitudes of phonon operators spread over many two-quasiparticle states. For example, the large E2 transitions for the β-, γ-vibrations or the wobbling motion under discussions are related to the first one, and the assumption (4.32) is justified by the second one. Let us call the former the "large-transition" collectivity and the latter the "spread-over" collectivity. The shape-vibrational motions in the ground-state regions almost always possess both the collectivities.

[6] As has already been mentioned in Section 2, the correct geometry is not always realized in the RPA formalism because it is based on the semi-classical cranking picture. This is the reason why there is a difference of factor 4 between Eqs. (4.36) and (3.13b), and one must explicitly use $\boldsymbol{m} - g_{xx}\boldsymbol{I}$ rather than $\boldsymbol{m}$ in the M1 transition operator (4.35) so as to get the expressions of the B(M1) corresponding to those in the rotor model.

In our experience, the spread-over collectivity gets weaker in most cases for the RPA solutions excited on the vacuum with rotational aligned quasiparticles, e.g. the s-band, at higher spins. One of the reasons for this is that the pairing correlations are reduced by the blocking effects of the aligned particles [33]. In spite of the fact that the phonon amplitudes tend to concentrate somewhat on a few components, the large-transition collectivity can survive even at higher spins, since the energy lowering of the two-quasiparticle states make the RPA eigenenergy small and the backward amplitudes remain large.

The above discussion indicates that the M1 amplitude with using the microscopic M1 operator (4.34) is small for the typical spread-over collective RPA solutions. In fact a destructive interference occurs for the M1 operator, because amplitudes of this type of solution, which are of isoscalar quadrupole character, have many two-quasiparticle components with phases favourable to the E2 operator. Since the quadrupole-shape vibrations in non-rotating nuclei have RPA amplitudes which transfer the K quantum number by even units, the transition matrix elements for the M1 operator strictly vanish. This is well established for the γ-vibrational bands at low spins, where the M1 transitions are usually small. Therefore the $\Delta I = \pm 1$ transitions are E2 dominant in such cases. It should, however, be noticed that the spread-over collectivity of the RPA solutions are reduced at higher spins and then the properties of individual two-quasiparticle states, whose components are dominant in the RPA amplitudes, manifest themselves as an enhancement of the M1 amplitudes. We will see examples of such cases, where the M1 transitions are not negligible or even dominant, in the next section.

It should be mentioned that the fact that the backward amplitudes are large, e.g. their squared sum typically amounts to ≈ 0.4–0.6 for low-lying β-, γ-vibrations and the wobbling motions, indicates that the small-amplitude ansatz of the RPA is not always satisfied. This difficulty has been well-known for many years and we must use a more elaborate theory to avoid this; for example, the nuclear-field theory, the boson mapping theory or the generator coordinate theory (see e.g. Ref. [34]). This is out of the scope of this paper.

5. Examples of numerical calculations

In the microscopic RPA formalism we have solutions of a vibrational character in many cases. As has been clarified in the previous sections, however, all of the solutions cannot necessarily be interpreted as wobbling-like motion even though they are collective enough in the sense that the E2 transition amplitudes are large (see discussion below Eq. (4.31)). Namely, in addition to enough collectivity, the relative sign of the transition amplitudes $\mathcal{Q}_y(n)$ and $\mathcal{Q}_z(n)$ should be the same as that of the static asymmetries around the y- and z-axes, i.e. α_y and α_z:

$$\text{sign of } \mathcal{Q}_y(n)/\mathcal{Q}_z(n) = \text{sign of } \alpha_y/\alpha_z. \tag{5.1}$$

This relation was expressed in another form in Eq. (4.9) of Ref. [28]. Only in such solutions the three moments of inertia associated with the RPA solutions, Eq. (4.22), are well-defined and are consistent with the picture of the wobbling motion. It is quite interesting that the lowest collective RPA solutions, when they exist, satisfy the condition in most of the cases we found. Eq. (5.1) even holds for γ-vibrational excitations in nuclei with small self-consistent γ deformation: It is a good approximation to set $\gamma = 0$ in such nuclei, and then the same relative sign as the self-consistent triaxiality (Eq. (5.1)) is obtained for the transition amplitudes even with such an artificial setting as $\gamma = 0$.

More precisely speaking, one must require the conditions Eq. (4.21) in order that the adopted small-amplitude approximation is valid. This means that both of the static deformations around y- and z-axes should be larger than the dynamic ones. One might therefore expect the ideal wobbling motion only in the region of equilibrium shape of $\gamma \neq 0°$ and $\gamma \neq -60°$ in the (ϵ_2, γ)-plane; i.e. an appreciable amount of triaxiality is generally required. Notice that the wobbling-like solutions can exist in the axially symmetric cases of $\gamma = 60°$ and $-120°$, where $\alpha_y = \alpha_z < 0$ and > 0, respectively, and correspond to the $\Delta I = 1$ excitations on a high-K isomer states (the precession bands) as is discussed at the end of Section 3.

This apparent asymmetry between the four cases of axially symmetric shapes is based on the fact that the three rotation axes are not equivalently treated; the x-axis is the main rotation axis and the angular momenta around the other two axes are small compared to it. This is generally believed to be valid near the yrast states. Such a treatment makes sense especially in the situation where the quasiparticle alignments occur. Then an appreciable part of the main rotation is carried by single-particle degrees of freedoms, while the perpendicular components of the rotation are only of a collective nature. Actually, we have found the wobbling-like solutions only in the cases where aligned quasiparticles exist in the vacuum state from which the RPA modes are excited, which causes the time-reversal violation of the vacuum and induces strong rotational K-mixing effects.

Keeping the general considerations stated above in mind, we will show some examples of the results of realistic calculations and discuss the characteristic properties of the obtained wobbling motions.

5.1. $\Delta I = \pm 1$ interband E2 transitions

Since we restrict ourselves to even–even nuclei, the yrast band under consideration naturally has the quantum numbers $(\alpha, \pi) = (0, +)$ with even-spin values. Then the (one-phonon) wobbling band has $(\alpha, \pi) = (1, +)$ with odd-spin values. Unfortunately, there are only a few cases where $(\alpha, \pi) = (1, +)$ bands are observed up to high-spin states. Moreover, it is generally difficult to distinguish the collective-phonon band from non-collective-quasi-particle bands, like the AC or BD two-neutron aligned bands in the usual nomenclature of quasiparticle orbits, only from the energy spectra. Thereby, until now, there is no definite evidence that the ideal wobbling motions exist in atomic nuclei.

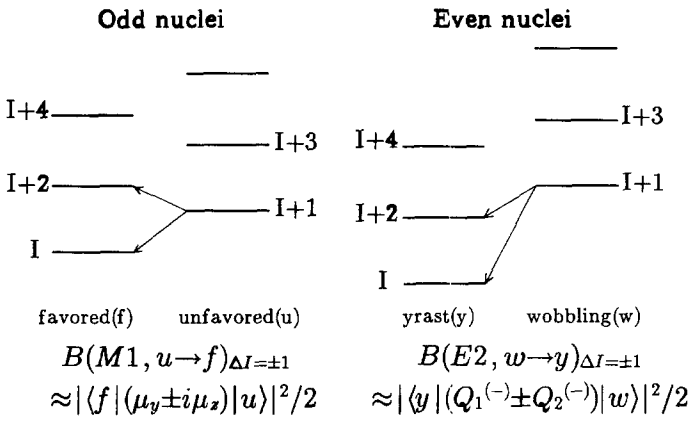

Fig. 2. Schematic figure depicting the analogy between the $\Delta I = \pm 1$ E2 transitions from the wobbling to the yrast band in even–even nuclei and the M1 transitions between the signature-partner bands in odd nuclei.

One of the most important features of the wobbling motions is that the E2 amplitudes $\mathcal{Q}_y(n)$ and $\mathcal{Q}_z(n)$ have comparative magnitude, in contrast to the case of the γ-vibrations in Section 2, where $|\mathcal{Q}_y(=t[Q_1^{(-)}])| \ll |\mathcal{Q}_z(=-t[Q_2^{(-)}])|$. This property immediately leads us to the fact that the one transition with either $\Delta I = +1$ or -1 is much larger than the other depending on the relative phase of $\mathcal{Q}_y(n)$ and $\mathcal{Q}_z(n)$ (see Eq. (4.2b)) or on the triaxiality (see Eq. (5.1)). This situation is quite analogous to that of the M1 transitions between the signature-partner bands in odd nuclei; the single-particle matrix elements of the operators $i\mu_y$ and μ_z between the signature-partner bands play a similar role as the two amplitudes $\mathcal{Q}_y$ and $\mathcal{Q}_z$ as is shown in Fig. 2, although the role played by the triaxiality is not necessarily the same. For the ideal case of the wobbling motion where the formula of the macroscopic model is valid, the staggering of the E2 transitions between $\Delta I = +1$ and -1, together with the excitation energies, gives important information on the triaxial deformation and/or the three moments of inertia; for example, the relation

$$\frac{\Delta B(\mathrm{E2})_{|\Delta I|=1}}{B(\mathrm{E2})_{|\Delta I|=2}} \equiv \frac{B(\mathrm{E2})_{\Delta I=-1} - B(\mathrm{E2})_{\Delta I=+1}}{B(\mathrm{E2})_{|\Delta I|=2}} = \frac{8}{I}\frac{\alpha_y \alpha_z}{(\alpha_y - \alpha_z)^2} \qquad (5.2).$$

can be used in a similar kind of analysis for the staggering of the M1 transitions in odd nuclei as seen in Ref. [35]. The relation between the $B(\mathrm{E2})_{\Delta I=\pm 1}$ and the triaxial-equilibrium deformation is summarized in Fig. 3. It should be mentioned that the model-independent analysis by means of the Coulomb-excitation technique (see e.g. Ref. [36]) gives important information on the magnitude of the triaxiality, but it cannot distinguish the three regions in Fig. 3 since only the invariant quantity $\cos(3\gamma)$ is extracted from such an analysis. The quantity like Eq. (5.2) gives additional information on it.

Although there is no definite evidence, it is suggested in Ref. [28] that the odd-spin sequence of the so-called "extension of the γ-band" [37] after the g–s band crossing in ^{182}Os might be a candidate of the wobbling motion when being seen from the calculations of the same RPA formalism. It is instructive to show results of the

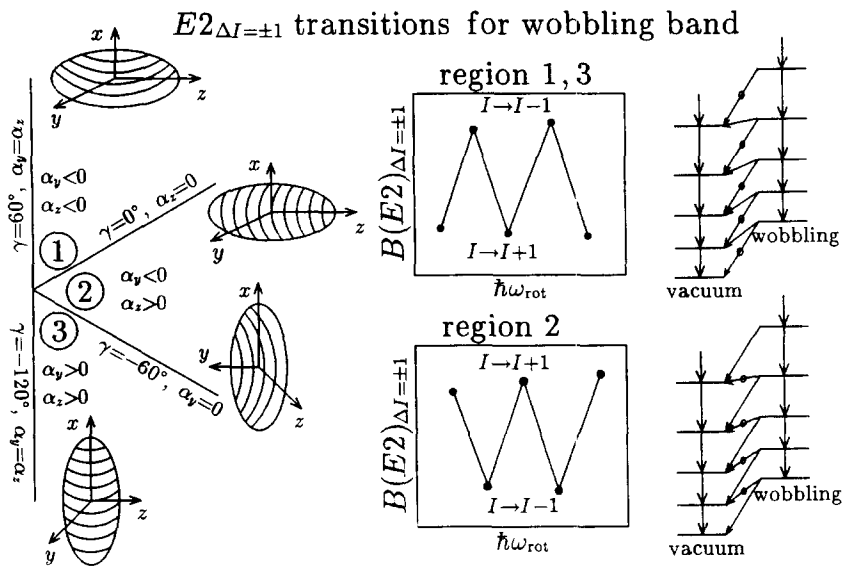

Fig. 3. Schematic figure depicting the relation between the triaxiality of the mean field and the zigzag behaviour of the $\Delta I = \pm 1$ E2 transitions from the wobbling to the vacuum band. The (ϵ_2, γ)-plane is divided into three regions, for which characteristic types of behaviour of $B(\mathrm{E2})_{\Delta I=\pm 1}$ are shown on the middle panels. The transitions with stronger B(E2)'s are marked in the spectra (right panels).

calculations for this nucleus because they exhibit such features as are expected from the discussions in the previous sections. This nucleus is supposed to be γ-soft and the two-quasineutron alignment induces the negative-γ deformation. The potential-energy surfaces are so flat that it is difficult to determine the precise γ-value. We have taken $\gamma = -18°$, since then the RPA results have desired properties like an ideal wobbling motion [15,28]. It should be stressed that, in order to obtain the wobbling-like RPA solution, the existence of the aligned quasiparticles in the vacuum configuration, e.g. the s-band, is indispensable.

The calculational procedures, i.e. the single-particle potential, the effective interactions, the model space, etc., are the same as those in Section 2. It should, however, be emphasized that the RPA dispersion equation, with the NG modes being explicitly decoupled [19], is used in this calculation. For the case of $\gamma \neq 0°$, the two quadrupole force parameters, $\chi_1^{(-)}$ and $\chi_2^{(-)}$, can be eliminated in the RPA equation for the signature $(-)$ sector by making use of the decoupling conditions of the NG modes. Therefore the wobbling-like RPA solutions are obtained without any ambiguity depending on the choice of the force parameters. All the mean-field parameters are fixed, with the values $\Delta_\nu = 0.74$ MeV, $\Delta_\pi = 0.98$ MeV and $\epsilon_2 = 0.21$, $\gamma = -18°$, just as in Ref. [28] [7]. These values are reasonable for the s-band of ^{182}Os. The results of the RPA

[7] In Refs. [15,28], the transition amplitudes are (10–30)% different because a larger model space ($N_{\rm osc}$ = 5–7 for neutrons and 4–6 for protons) from that adopted in this paper has been used. From the results in Section 2 we hope that the calculations in this paper are more appropriate. In addition, the results in Ref. [28] were obtained by using the RPA equation in which the NG modes are not explicitly decoupled.

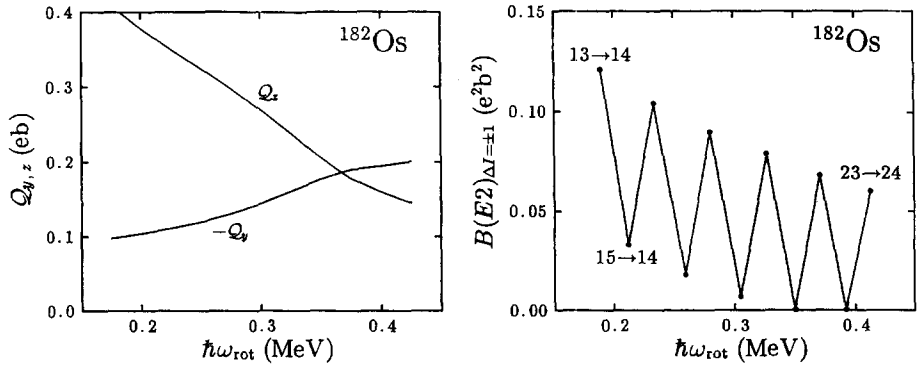

Fig. 4. The E2 transition amplitudes, $\mathcal{Q}_y$ and $\mathcal{Q}_z$ (left panel) and $\Delta I = \pm 1$ B(E2) (right panel), for the lowest $\alpha = 1$ RPA solution as functions of the rotational frequency in ^{182}Os. The mean-field parameters are fixed as $\epsilon_2 = 0.21$, $\gamma = -18°$ and $\Delta_\nu = 0.74$ MeV, $\Delta_\pi = 0.98$ MeV, which are appropriate for the s-bands in ^{182}Os [28]. As a reference the Weisskopf unit of B(E2) in this case is 0.0061 e^2b^2.

amplitudes for the lowest RPA solution and the corresponding B(E2)-values are shown as functions of the rotational frequency in Fig. 4. Since $-60° < \gamma < 0°$, $\alpha_y < 0$ and $\alpha_z > 0$, the relative sign of $\mathcal{Q}_y(n)$ and $\mathcal{Q}_z(n)$ for the solution is negative (see Eq. (5.1)). Thus the transition from $(I-1)_{\rm wob}$ to $(I)_{\rm s}$ is much stronger than the one from $(I+1)_{\rm wob}$ to $(I)_{\rm s}$, as is clear in Fig. 4 (see also Fig. 3). Accordingly the B(E2) values show remarkable zigzag behaviour.

Unfortunately these transition rates have not yet been measured. Since the γ-ray energy for the $(I-1)_{\rm wob} \to I_{\rm s}$ transition is much smaller, the γ-decay rate for this transition is hindered although the B(E2)-values are large. This might be the reason why it is difficult to measure the transitions. As is clear from the general consideration, if the wobbling-type RPA solution exists for the positive-γ equilibrium shape, the relative sign of $\mathcal{Q}_y(n)$ and $\mathcal{Q}_z(n)$ is positive and then both the B(E2) and the γ-ray energy for the $(I+1)_{\rm wob} \to I_{\rm s}$ transition is larger. It might, therefore, be more easy to measure the transitions in this case, although we could not find a good example of such calculations.

The M1 transitions between the wobbling and the s-band in this nucleus are small; typically $B(\mathrm{M1})(\mu_N^2)/B(\mathrm{E2})(e^2b^2) \approx 0.1$, except for the highest frequency where the M1 amplitudes start to grow rapidly (not shown). The smallness of the M1 amplitudes comes from the fact that the wobbling solution in this nucleus has a characteristic collectivity discussed at the end of Section 4 which remains large up to rather high spins, although it gradually decreases as a function of the rotational frequency (see the B(E2)-values in Fig. 4).

Finally, it should be mentioned that the second RPA solution in this nucleus is also considerably collective [28]. However, the relative sign of $\mathcal{Q}_y(n)$ and $\mathcal{Q}_z(n)$ is positive and therefore it is a kind of vibrational mode but not of a wobbling nature.

5.2. Effective moments of inertia

Another important outcome of the microscopic RPA formalism is that the three effective moments of inertia [2] can be calculated, which is highly non-trivial from the microscopic viewpoint. It should be noticed that the ratios $\mathcal{J}_y^{\rm eff}(n)/\mathcal{J}_x$ and $\mathcal{J}_z^{\rm eff}(n)/\mathcal{J}_x$ can be extracted from the ratios $\omega_n/\omega_{\rm rot}$ and $\mathcal{Q}_y(n)/\mathcal{Q}_z(n)$ through Eqs. (4.26) and (4.29); the latter two are experimentally observable from the energy spectra and the $B(\mathrm{E2})_{|\Delta I|=1}/B(\mathrm{E2})_{|\Delta I|=2}$. It may, therefore, be interesting to see how the three moments of inertia calculated from the wobbling RPA solution behave as functions of deformation parameters, especially the triaxiality γ. Their dependence on the rotational frequency has already been studied in Ref. [28] for ^{182}Os and will be presented for ^{124}Xe in the next subsection. In the case of the quadrupole residual interaction, a simple formula for $\mathcal{J}_{y,z}^{\rm eff}(n)$ in terms of the 2×2-coupled RPA dispersion equations exist [19,28]. We use this formula in the following calculations in place of the original definition, Eq. (4.22).

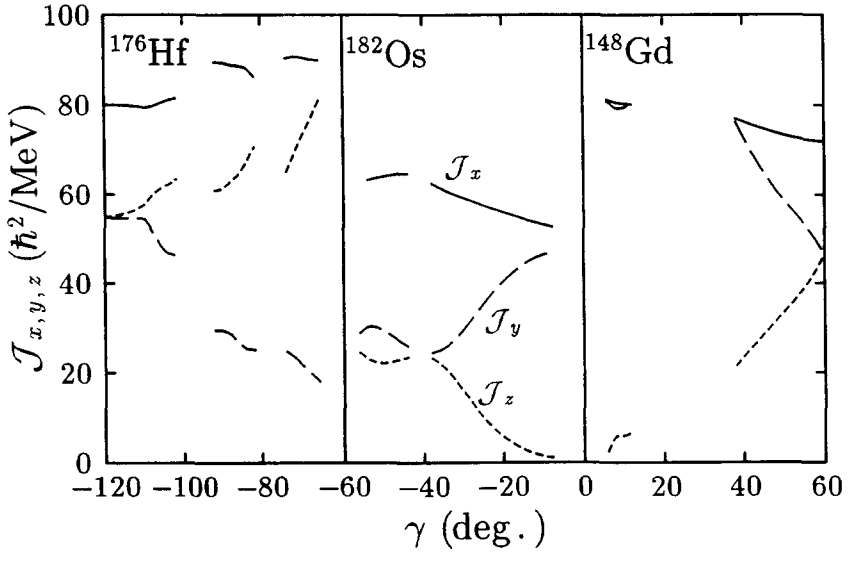

Fig. 5. The effective moments of inertia as functions of the triaxial parameter γ at $\hbar\omega_{\rm rot}=0.25$ MeV. The results for $-120°<\gamma<-60°$ in ^{176}Hf, for $-60°<\gamma<0°$ in ^{182}Os and for $0°<\gamma<60°$ in ^{148}Gd are combined in one figure. The mean-field parameters except for γ are fixed as $\epsilon_2=0.27$ and 0.22 for ^{176}Hf and ^{148}Gd, respectively, and $\Delta_\nu=\Delta_\pi=0.6$ MeV for both nuclei. The same parameters as in Fig. 4 are used for ^{182}Os. Note that ^{176}Hf and ^{148}Gd are known to be nuclei with prolate and oblate non-collective rotations so that the self-consistent γ deformations are $\gamma=-120°$ and 60°, respectively. The diabatic configurations of the vacuum states are chosen to be a two-quasineutron, four-quasiproton state for ^{176}Hf, a two-quasineutron state (s-band) for ^{182}Os, and a two-quasineutron and two-quasiproton state for ^{148}Gd. For ^{176}Hf and ^{148}Gd, these configurations correspond to the high-K states with $K^\pi=20^+$ and 18^+, respectively, which are yrast states with $(\pi,\alpha)=(+,0)$ for both neutron and proton at their self-consistent deformations. Unfortunately these high-K states do not coincide with any of the observed yrast isomers.

Of course the triaxiality of the equilibrium shape is determined by the energy minimization in the (ϵ_2, γ)-plane. Instead, we fixed the other parameters of the mean-field potential and have performed the RPA calculations changing the γ-deformation as a free parameter. Thus, such calculations should be considered to be a kind of theoretical simulation of how the nucleus behaves under the artificial change of the triaxiality. The results for the three sectors in the (ϵ_2, γ)-plane, i.e. $-120° < \gamma < -60°$, $-60° < \gamma < 0°$ and $0° < \gamma < 60°$ (see Fig. 3), in each of which we selected ^{176}Hf, ^{182}Os or ^{148}Gd as a typical example, respectively, are shown together on a panel in Fig. 5. Note that the yrast sequences of ^{176}Hf and ^{148}Gd are known to be composed of non-collective rotations with prolate and oblate shapes, i.e. $\gamma = -120°$ and 60°, respectively. Since all the other mean-field parameters are fixed by neglecting the self-consistency, the wobbling-like solutions are obtained not for all values of γ deformation, and, moreover, the solutions can be discontinuous as functions of γ because of the existence of virtual level crossings of the quasiparticle orbits when changing γ.

In spite of deficiencies of these relatively simple-minded calculations, it is instructive to see the *microscopically derived* γ-dependence of the three moments of inertia, which is neither irrotational-like nor rigid-body-like. In these calculations all the vacuum states, on which the RPA mode excited, have aligned quasiparticles, which is essential to obtain the wobbling-like solutions as is mentioned above, so that the $\mathcal{J}_x = I/\hbar\omega_{\rm rot}$ (kinematical moment of inertia) changes very gradually and never vanishes. Thus the γ-dependence of the three moments cannot be that of irrotational ones. On the other hand, $\mathcal{J}_k^{\rm eff}$ $(k = y, z)$ are dynamical moments of inertia and take as small values as zero. Thus the γ-dependence of the three moments cannot be that of a rigid-body, either.

It is very interesting to see how the three moments of inertia, which can be experimentally extracted from the observed wobbling motions, if they exist, behave. For this purpose, the triaxial deformation should also be determined from the independent experimental observables, e.g. from the M1 transitions in neighbouring nuclei.

5.3. *Wobbling motion in ^{124}Xe*

As pointed out above, one of possible candidates of wobbling motion is the high-spin continuation of the odd-spin members of the so-called γ-band. Actually a scenario of character change from the γ-vibrational to the wobbling-like band was first pointed out in Ref. [7], and such a trend, though not developed well because of the small triaxiality, was suggested for ^{164}Er in Ref. [19]. The essential point is that a structural change of the vacuum caused by the quasiparticle alignment transfers an appreciable amount of $K = 1$ quadrupole strength from the Nambu–Goldstone mode to the normal modes. Although it is difficult to predict precisely in which nuclei a wobbling mode appears, because this mode is an outcome of a subtle interplay between rotation, quadrupole and pairing correlations in realistic nuclei, we have at least up to now two typical candidates of wobbling motion in observed bands with negative γ-deformation: One is in ^{182}Os after the $(\nu i_{13/2})^2$ alignment discussed in Ref. [28] and above, and the other is in ^{124}Xe [38]

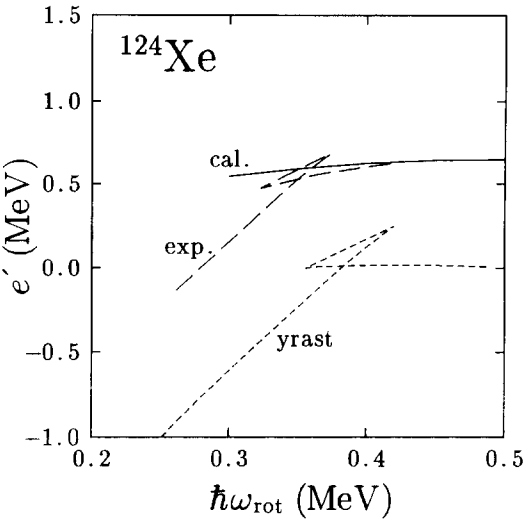

Fig. 6. Routhians for the lowest-lying $\alpha = 1$ bands as functions of the rotational frequency in ^{124}Xe. The calculated one is shown by the solid line, the experimental one, which is the routhian of the odd-spin members of the so-called γ-band, by the dashed line, and the observed yrast band by the short-dashed line. Experimental routhians are shown with respect to a reference band with $\mathcal{J}_0 = 15.0\ \hbar^2/\text{MeV}$, $\mathcal{J}_1 = 25.0\ \hbar^4/\text{MeV}^3$, $e_s = 3.03$ MeV and $i_s = 7.14\ \hbar$. Parameters used in the calculation are $\epsilon_2 = 0.19$, $\gamma = -45°$ and $\Delta_\nu = 0.9$ MeV, $\Delta_\pi = 1.1$ MeV.

after the $(\nu h_{11/2})^2$ alignment, being discussed in the following [8]. An important characteristic common to both nuclei is that the low-spin spectrum is almost rotational but relatively γ-soft, while the negative γ-deformations, i.e. $-30° < \gamma < 0°$ in ^{182}Os and $-60° < \gamma < -30°$ in ^{124}Xe, are stabilized above the first band crossing caused by the high-Ω quasiparticles. Here we note that in ^{182}Os the γ-rays which link (the candidate of) the odd-spin members of the γ-band above and below the band crossing have not been observed. From this fact, we imagine that it might well be the case that there might exist wobbling-like bands but that they have been assigned incorrectly as non-collective two-quasiparticle bands in other nuclei because of the lack on the linking transitions. A possible mechanism of this situation will be discussed later in Subsection 5.4 for the case of ^{126}Ba.

The low-spin nuclear structure of Xe isotopes has been studied extensively by means of the interacting-boson model [39] and known to depend smoothly on the neutron number. A recent study [40], however, pointed out that above the first band crossing there are some properties which show sudden changes between $A = 120$ and 122 due to the shape coexistence; the lighter isotopes remain nearly axially symmetric while the heavier ones become triaxial with $\gamma < 0$. In particular, in ^{120}Xe, a candidate of the even-spin continuation of the γ-band above the *second* band crossing has been found for the first time, whereas in ^{124}Xe, the odd-spin sequence has been known to extend up to

[8] We thank Ramon Wyss for informing us of these data.

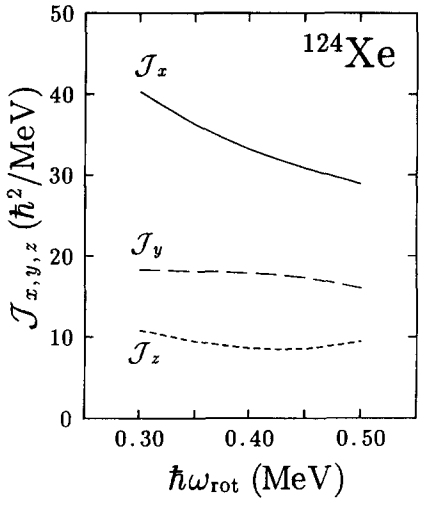

Fig. 7. Calculated effective moments of inertia for the lowest $\alpha = 1$ RPA solution in ^{124}Xe as functions of the rotational frequency. The parameters used are the same as in Fig. 6.

higher spins than the even-spin one [38] and it shows a well-developed wobbling character. We mainly concentrate on ^{124}Xe in the following, although similar results can be obtained for other isotopes with similar triaxial deformation.

The result of the RPA calculation for ^{124}Xe based on the $(\nu h_{11/2})^2$ aligned configuration is shown in Fig. 6 together with the experimental routhians relative to a reference which makes the routhian of the s-band flat. The method of calculation is the same as that in the previous sections, but the smaller model space with $N_{\rm osc} = 3$–5 for both neutrons and protons are used in this region of nuclei. This calculation has been done using the deformation parameters $\epsilon_2 = 0.19$ and $\gamma = -45°$, which are taken from the total-routhian-surface (TRS) calculation at $\hbar\omega_{\rm rot} = 0.3$ MeV in Ref. [41]. The hexadecapole deformation is neglected for simplicity. Although the meaning of the shape parameters is slightly different because of the different single-particle potential adopted in Ref. [41], we confirmed the stability of results of our calculations against a possible small change of shape parameters. The pairing gaps $\Delta_\pi = 1.1$ MeV and $\Delta_\nu = 0.9$ MeV which are typical for the low-spin part of the neutron s-bands in this region are used. This RPA calculation reproduces the data very well. Note, again, that we do not have any adjustable parameter in the step of RPA for the signature $(-)$ sector. Calculated effective moments of inertia are shown in Fig. 7. They vary as functions of the rotational frequency in spite of the fact that the nuclear shape is fixed as in the case of ^{182}Os [28] but the dependence is much weaker in ^{124}Xe.

Calculated E2 and M1 transition amplitudes are shown in Fig. 8 and 9, respectively, as functions of the rotational frequency, where the standard values of g_l and $g_s^{(\rm free)}$ [42], and $g_s^{(\rm eff)}/g_s^{(\rm free)} = 0.7$ are used in this and the following calculations for the M1 operators (4.35). In the figures, the transition probabilities are also included. Since the self-consistent $\gamma = -45°$, the relative phase between $\mathcal{Q}_y$ and $\mathcal{Q}_z$ is negative so that the

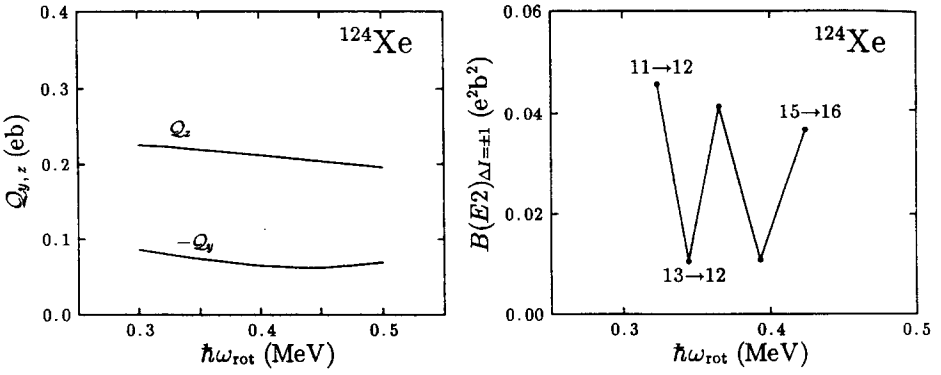

Fig. 8. The E2 transition amplitudes, $\mathcal{Q}_y$ and $\mathcal{Q}_z$ (left panel) and $\Delta I = \pm 1$ B(E2) (right panel), for the lowest $\alpha = 1$ RPA solution as functions of the rotational frequency in ^{124}Xe. The parameters used are the same as in Fig. 6. As a reference the Weisskopf unit of B(E2) in this case is 0.0037 e^2b^2.

$\Delta I = +1$ transitions are stronger in the same way as in ^{182}Os. It is, however, noticed that the collectivity of the RPA solution, especially the spread-over one, is weaker than that in ^{182}Os, and consequently the M1 transition is stronger in ^{124}Xe. Actually, as is seen from Figs. 8 and 9, M1 transitions can compete with E2 depending on the transition energies. The zigzag behaviour of the E2 and M1 transitions is the same in this case (see Figs. 8 and 9). It might be interesting to point out that the trend that the E2 transitions decrease against the spin while the M1 transitions increase coincides with the prediction of the macroscopic rotor model in this case (see Eqs. (3.7b) and (3.13c)).

We use the quadrupole residual interaction which has two components, $K = 1$ and $K = 2$, in the signature $(-)$ sector. It should be noted that a triaxial deformation mixes the K quantum number by two units so that the $K = 1$ and 2 components of the interaction couple only through the rotational motion. What brings about the character

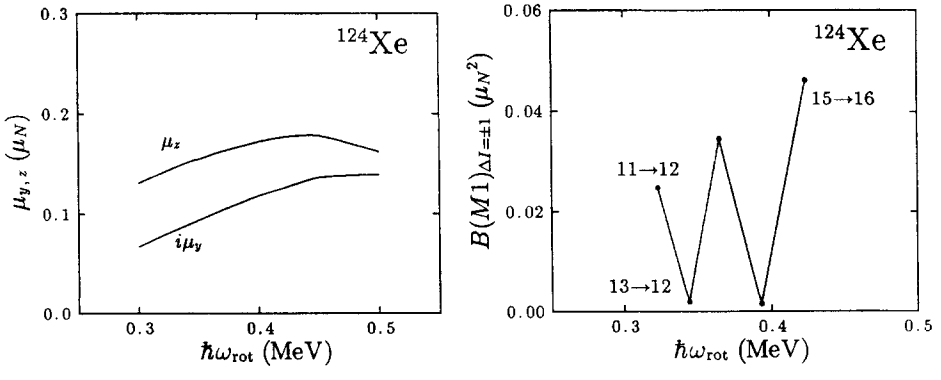

Fig. 9. The M1 transition amplitudes, $i\mu_y$ and μ_z (left panel) and B(M1) (right panel), for the lowest $\alpha = 1$ RPA solution as functions of the rotational frequency in ^{124}Xe. Note that the relative phase between the M1 amplitudes and the E2 amplitudes (Fig. 8) is meaningful and gives the sign of the E2/M1 mixing ratio. The parameters used are the same as in Fig. 6. As a reference the Weisskopf unit of B(M1) is 1.79 μ_N^2.

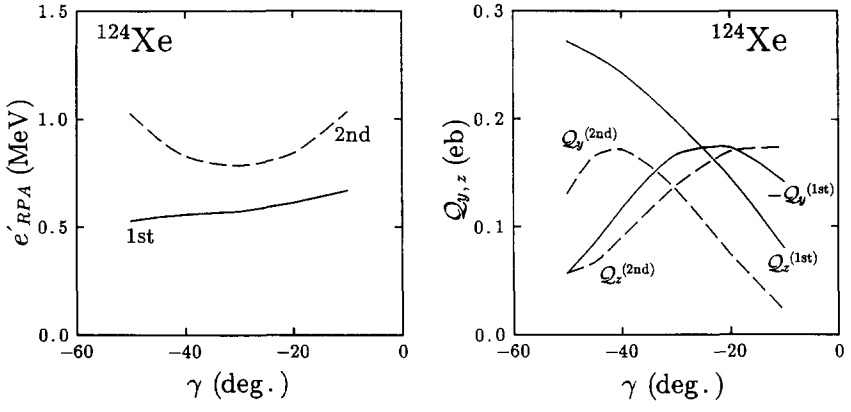

Fig. 10. Excitation energies (left panel) and the E2 transition amplitudes (right panel) for the lowest and second-lowest $\alpha = 1$ states in ^{124}Xe calculated at $\hbar\omega_{\rm rot} = 0.3$ MeV as functions of γ. The parameters used, except for γ, are the same as in Fig. 6.

change of the lowest collective excitation is the interplay of these two components intermediated by the rotational coupling. To look at this mechanism more closely, it is useful to see the second-lowest RPA solution together with the lowest one that we have been discussing. The excitation energies of the two solutions and the $K = 1$ and 2 quadrupole transition amplitudes, $\mathcal{Q}_y (= t[Q_1^{(-)}])$ and $\mathcal{Q}_z (= -t[Q_2^{(-)}])$, associated with them, calculated at $\hbar\omega_{\rm rot} = 0.3$ MeV, are shown in Fig. 10 as functions of γ from $-60°$ to $0°$. The calculations have been done using the same mean-field parameters (except γ) as in Fig. 6. The second-lowest solution shares an appreciable amount of $\mathcal{Q}_y(n)$ and $\mathcal{Q}_z(n)$ strength with the lowest one but with the different relative sign between them. We have already encountered a similar situation in the case of ^{182}Os [28]. In order to interpret these results, we consider the axially symmetric limits, $\gamma = 0°$ and $-60°$, where the symmetry axes are the z- and y-axes, respectively. Since the roles of the y-and z-axes are interchanged (with the rotation axis unchanged) in both cases, the modes with $|\mathcal{Q}_z| \gg$ (or $\ll$) $|\mathcal{Q}_y|$ in $\gamma = 0°$ on the one hand correspond to those with $|\mathcal{Q}_y| \gg$ (or $\ll$) $|\mathcal{Q}_z|$ in $\gamma = -60°$ on the other hand. We can see clearly in Fig. 10 that this correspondence actually holds and, moreover, that the strongest K-mixing of the two amplitudes occurs around $\gamma = -30°$. Let us call the mode with $|\mathcal{Q}_z| \gg |\mathcal{Q}_y|$ in $\gamma = 0°$ "γ-vibration-like"; then so is the second-lowest solution in ^{124}Xe at the rotational frequency shown. In contrast, the lowest solution in ^{182}Os is "γ-vibration-like" at $\hbar\omega_{\rm rot} \lesssim 0.25$ MeV as is shown in Fig. 4. It should, however, be noticed that the lowest solution follows the "phase rule" (5.1), which allows us to interpret the lowest solution as a wobbling motion in both the cases. According to the previous discussions, the $\Delta I = +1$ E2 transitions are larger for the lowest solution because $\mathcal{Q}_y/\mathcal{Q}_z < 0$, while the $\Delta I = -1$ E2 transitions are larger for the second-lowest solution. No candidate for the second-lowest collective excitation has been observed so far. According to the TRS calculation [41] the equilibrium shape of the $(\nu h_{11/2})^2$ band of ^{122}Xe is $\gamma \simeq -30°$, where the excitation energy of the second-lowest solution becomes low and the

difference between $B(E2)_{\Delta I=\pm 1}$ becomes conspicuous due to the K-mixing. So we think ^{122}Xe is a more promising nucleus for which our theoretical prediction can be tested.

5.4. Continuation of the γ-band in ^{126}Ba

Next we study the high-spin continuation of the γ-band in ^{126}Ba [43]. This nucleus is also relatively γ-soft at low spins, while the first band crossing is caused by the low-Ω $(\pi h_{11/2})^2$ in contrast to the isotone ^{124}Xe studied above. See Fig. 6 of Ref. [41] for a summary of the data. The alignment of high-j and low-Ω quasiparticles drives the nucleus towards $\gamma \gtrsim 0$. We have performed the RPA calculation for excitations on top of the $(\pi h_{11/2})^2$ configuration adopting $\epsilon_2 = 0.24$ and $\gamma = 0$ according to the TRS calculation [43] just as in the case of ^{124}Xe. On the other hand, the pairing strengths are chosen so as to reproduce their band-crossing frequencies (see Fig. 12 of Ref. [43]) for both proton ($\hbar\omega_c \simeq 0.35$ MeV) and neutron ($\simeq 0.44$ MeV) when the gap self-consistent calculation has been done. We also confirmed that the parameters thus adopted reproduce the experimental data even near the ground state; for example, the observed $B(E2; 2_1^+ \to 0_1^+) = 1.9 \pm 0.2\ e^2b^2$. The calculated pairing gaps for the proton s-band are $1.16 \geqslant \Delta_\nu \geqslant 1.03$ MeV and $0.76 \geqslant \Delta_\pi \geqslant 0.71$ MeV for $0.4 \leqslant \hbar\omega_{rot} \leqslant 0.5$ MeV. Since $\gamma \approx 0°$ in this case we cannot use the RPA equation with the NG modes fully decoupled. We therefore have used the equation with the NG modes partially decoupled [19], which is suitable for $\gamma = 0°$, where the force parameter $\chi_2^{(-)}$ is not eliminated from the RPA equation. The $\chi_2^{(-)}$ in this case has been fixed so as to give the correct excitation energy of the γ-vibration on the ground state as $\hbar\omega_\gamma(\hbar\omega_{rot} = 0) = 0.873$ MeV.

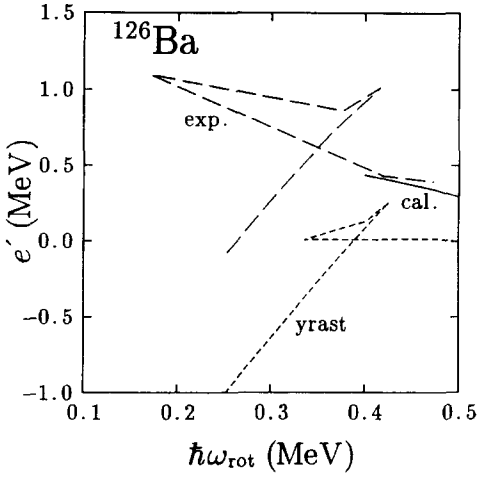

Fig. 11. The same as Fig. 6 but for ^{126}Ba. The deformation parameters used are $\epsilon_2 = 0.24$, $\gamma = 0$, and the self-consistently calculated pairing gaps are $1.16 \geqslant \Delta_\nu \geqslant 1.03$ MeV and $0.76 \geqslant \Delta_\pi \geqslant 0.71$ MeV for $0.4 \leqslant \hbar\omega_{rot} \leqslant 0.5$ MeV. A reference band with $\mathcal{J}_0 = 14.0\ \hbar^2/\text{MeV}$, $\mathcal{J}_1 = 31.0\ \hbar^4/\text{MeV}^3$, $e_s = 3.00$ MeV and $i_s = 7.64\ \hbar$ is used. Note that the γ-ray which links above and below the band crossing has not been observed (see the text).

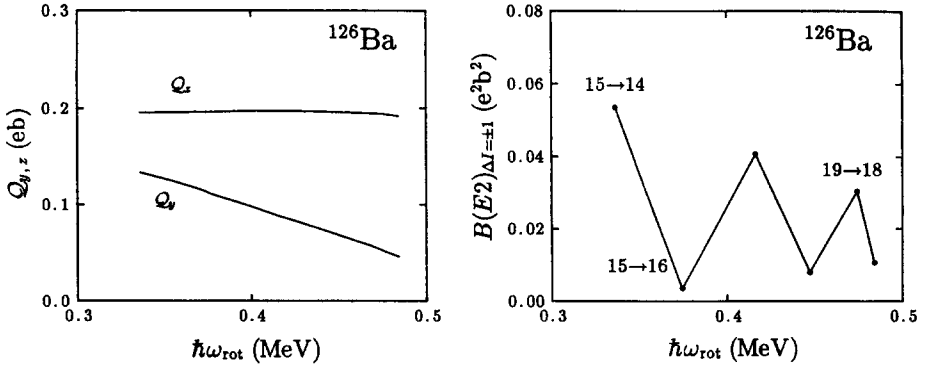

Fig. 12. The same as Fig. 8 but for ^{126}Ba. The parameters used are the same as in Fig. 11. As a reference the Weisskopf unit of B(E2) in this case is 0.0038 e^2b^2.

The result of the calculated routhian is shown in Fig. 11 together with the data seen from a reference which makes the routhian of the s-band flat, while the E2 and M1 amplitudes are depicted in Figs. 12 and 13 with the corresponding transition probabilities included. The excitation energy decreases as the rotational frequency increases both in the data and the calculation; this is contrary to the macroscopic wobbling motion. This result, together with the fact that the calculated signature splitting of energy between the $\alpha = 0$ (not shown) and $\alpha = 1$ RPA solutions is very small, favours an interpretation that the band under consideration remains to be γ-vibration-like rather than evolving to wobbling-like above the band crossing, as in the case of ^{164}Er [19]. In fact, the mixing of the $K = 1$ component is not so strong, as is shown in Fig. 12, which supports this interpretation. The collectivity measured by the sum of the squared backward amplitudes is similar to the ^{124}Xe case; ~ 0.6 in both nuclei. Consequently the magnitudes of the interband B(E2) are also similar, although the $\Delta I = -1$ B(E2) is now larger than the $\Delta I = +1$ one because $\mathscr{Q}_y/\mathscr{Q}_z > 0$, which is characteristic of small positive-γ nuclei (see Eq. (5.1)). This trend of the triaxiality reflects the shape-driving effect of the low-Ω aligned $(\pi h_{11/2})^2$. The zigzag behaviour of the M1 transitions is

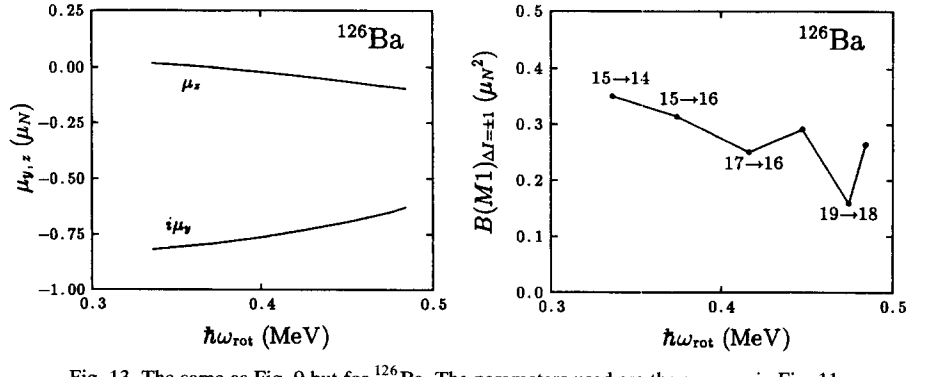

Fig. 13. The same as Fig. 9 but for ^{126}Ba. The parameters used are the same as in Fig. 11.

not pronounced at all in this case. This is because the μ_z-amplitudes are very small. In addition, the M1 transition is decreasing as a function of the rotational frequency, which is in contradiction with the prediction of the macroscopic formula.

An interesting feature of the data in this ^{126}Ba nucleus is that two branching ratios for decays from the members of the band under consideration, $T(17^+_{s\gamma} \rightarrow 16^+_s)/T(17^+_{s\gamma} \rightarrow 15^+_{s\gamma})$ and $T(19^+_{s\gamma} \rightarrow 18^+_s)/T(19^+_{s\gamma} \rightarrow 17^+_{s\gamma})$, where s and s$\gamma$ stand for the s-band and the $\alpha = 1$ γ-band excited on top of the s-band, respectively, were measured. Using the calculated values B(E2: $I_{s\gamma} \rightarrow (I-1)_s) = 0.044\ e^2b^2 = 12$ W.u. (cf. Fig. 12) and B(E2: $I_{s\gamma} \rightarrow (I-2)_{s\gamma}) \simeq B$(E2: $(I-1)_s \rightarrow (I-3)_s) = 0.69\ e^2b^2 = 184$ W.u. at $\hbar\omega_{rot} = 0.4$ MeV and measured γ-ray energies, the estimated branching ratio is T(E2: $I_{s\gamma} \rightarrow (I-1)_s)/T$(E2: $I_{s\gamma} \rightarrow (I-2)_{s\gamma}) \sim 0.05$, which is an order of magnitude smaller than the measured one [43]. This apparent contradiction between experiment and calculation can be solved by the specific property of the RPA solution in such a case as this, where the M1 transition is very strong, as is shown in Fig. 13. Compare the B(M1)-values with those of ^{124}Xe in Fig. 9.

As is pointed out above, the collectivity of the calculated solution in this case is more or less similar to that in ^{124}Xe, which is a little bit weaker than that in ^{182}Os. Actually, looking into the details of the microscopic structure of the RPA phonon, we have found an appreciable amount of concentration of the phonon amplitudes to the two-quasiparticle components with $(\pi h_{11/2})^2$ in ^{126}Ba and with $(\nu h_{11/2})^2$ in ^{124}Xe, in contrast to the strong spread-over collectivity seen in the case of ^{182}Os. The concentration to the different orbits in ^{126}Ba and ^{124}Xe comes from the fact that the aligned quasiparticles in the vacuum configurations are protons in the former and neutrons in the latter, and then clearly explains why the M1 transition is of an order of magnitude stronger in ^{126}Ba than in ^{124}Xe (note also that the amount of concentration in the former is a little bit stronger than in the latter). In fact the value B(M1: $I_{s\gamma} \rightarrow (I-1)_s) = 0.28\ \mu_N^2 = 0.15$ W.u. calculated at $\hbar\omega_{rot} = 0.4$ MeV (cf. Fig. 13) explains the observed branching ratio very well. We think, therefore, that these ^{126}Ba data are the first evidence of the rotationally induced "collective" M1 transition between the γ- and yrast bands in the sense that it has much larger M1 transitions than E2 transitions though it is an even–even nucleus.

This M1 matrix element on the other hand gives a possible explanation of why the linking transition between the sγ- and gγ-bands with $\alpha = 1$ was not observed. The calculated reduced transition rates for sγ to s give, e.g., T(M1) $= 0.23 \times 10^{13}$ s^{-1} and T(E2) $= 0.015 \times 10^{13}$ s^{-1} for $15_{s\gamma} \rightarrow 14_s$ ($E_\gamma = 0.781$ MeV). For the sγ-to-gγ transitions, it is difficult to estimate the effect of the g–s band crossing on them. If we assume a pure rotational E2 transition as if no band crossing would exist and use the same deformation in the g- and s-band, an upper limit may be obtained at T(E2) $< 0.005 \times 10^{13}$ s^{-1} for $15_{s\gamma} \rightarrow 13_{g\gamma}$ ($E_\gamma = 0.354$ MeV). Consequently the intensity of the sγ-band flows to the s-band rather than the gγ-band. Two mechanisms contribute to this result: i.e. the small transition energy in $I_{s\gamma} \rightarrow (I-2)_{g\gamma}$ and the large M1 transitions in $I_{s\gamma} \rightarrow (I-1)_s$. In the case of ^{182}Os with negative γ-deformation, however, these mechanisms do not seem to be applicable because E_γ ($9_{s\gamma} \rightarrow 8_s$) is also small and the M1 transition is hindered.

5.5. *Effects on properties of odd-A nuclei*

As has been discussed in the previous sections, the character of the lowest-lying collective excitations with $\alpha = 1$ is γ-vibration-like below the first band crossing while it sometimes acquires appreciable $K = 1$ quadrupole strength and therefore becomes wobbling-like above the band crossing. Rotational bands based on high-j one-quasiparticle configurations in odd-A nuclei decouple into a pair of $\Delta I = 2$ sequences labeled by the different signature quantum number. The vibrational excitation mode under consideration in even–even nuclei affects signature-dependent properties of adjacent odd-A nuclei through the particle-collective coupling [20]. We briefly summarize here the basic consequences of the dynamic coupling effects.

$B(\mathrm{E2}: I \to I - 1)$, connecting these two sequences, has been known to show signature-dependence, i.e., zigzag behaviour as a function of spin, which has been observed experimentally in some one-quasiparticle bands [44,45] before the band crossing. The theoretical studies have revealed that the signature-dependence is brought about not only by the static [46] but also by the dynamic [47–49] triaxial deformations. These two effects usually contribute in opposite sign, and, for example, the effect of the dynamic one is partly canceled by that of the static one in ^{157}Ho [44], while the latter is dominant in ^{161}Dy [45]. This dynamic effect is nothing else but the manifestation of the $K = 2$ collectivity of the vibrational excitation considered in this paper and plays an important role in understanding the electromagnetic properties of odd-A nuclei.

Above the band crossing, i.e. in three-quasiparticle bands (e.g. $(\pi \mathrm{h}_{11/2})^1(\nu \mathrm{i}_{13/2})^2$) in odd-$A$ nuclei, the signature splitting of the excitation energy between the two sequences often becomes smaller than before the crossing and even becomes inverted in some cases; i.e. the so-called signature inversion. This phenomenon has been explained in a similar way to that for odd–odd nuclei [50–54] as a result of positive-γ deformation. But this mechanism is not appropriate to explain the inversion in the three-quasiparticle bands which has been supposed to have negative-γ deformation, for example, in the cases of ^{165,167}Lu [55]. One of the present authors showed that the phase rule (5.1) results in a stronger particle-collective coupling in the unfavoured ($I = j +$ odd) sector than in the favored ($I = j +$ even) sector in negative-γ nuclei and consequently causes signature inversion [56]. In this model the effect of the static triaxiality is usually stronger and therefore the explanation in Refs. [50–54] consistently survives for positive-γ nuclei. This example clearly shows, again, the importance of the collective vibrational modes in the high-spin spectroscopy.

6. Concluding remarks

We have studied the nuclear wobbling motion from a microscopic viewpoint paying special attention to the electromagnetic-transition properties, especially E2 and M1, and to their implications in relation with the macroscopic Bohr–Mottelson model. Our basic standpoint is the RPA theory suitable for high-spin states, which has been proposed by

Marshalek [2,17] and developed by the present authors [19,20]. In order to check the reliability of the microscopic framework, the rotational perturbation to the E2 transitions between the γ-vibrational and the yrast bands in the low-spin region has been examined. Bohr–Mottelson's generalized intensity relation naturally comes out, in which the intrinsic transition moments can now be calculated microscopically. The results of the calculations show that both the absolute magnitude and the relative phase of these moments are well reproduced for some typical rare-earth nuclei.

The strong rotational perturbation at high-spin states causes the structural change of the vacuum configuration, i.e. the quasiparticle alignments or the band crossings. Accordingly the vibrational-excitation modes are naturally expected to change their characters. In order to understand the character change, interpretations of the observable quantities are necessary. For this purpose the microscopic wobbling model [2] based on the RPA theory has been reinvestigated in the light of the macroscopic wobbling model [1]. It has been shown that the expressions not only of excitation energy, which have already been discussed in Ref. [2], but also of the electromagnetic-transition rates can be cast into a form similar to those given by the macroscopic rotor model. The $\Delta I = \pm 1$ E2 transitions are especially important and give us criteria to identify the wobbling motion among the RPA solutions: (1) it should be a collective solution, and (2) the relative sign of the dynamic quadrupole asymmetries around the axes perpendicular to the main rotation axis, i.e. the transition amplitudes $\mathscr{Q}_y(n)$ and $\mathscr{Q}_z(n)$ (see Eqs. (4.1) and (4.3)), has to be the same as that of the static asymmetry around each axis, α_y and α_z (see Eq. (3.8)). Just as in the rotor model, the wobbling frequency as well as the E2 transition depend on the three moments of inertia. Therefore the wobbling motion reflects the three-dimensional nature of the nuclear collective rotations as a whole.

The wobbling motion is a unique rotational motion in the sense that the rotation axis deviates from the inertia axis of the nuclear body. Recently, a similar rotation scheme, called "tilted-axis cranking" [57], was proposed and has been applied to the study of the rotational bands with no-signature splitting. Although both the rotations are of three-dimensional nature, they are conceptually different; the wobbling motion is not the stationary motion and the angular-momentum and the angular-frequency vectors draw different trajectories in the body-fixed frame, while the tilted cranking is the stationary rotation and then the angular-momentum and angular-frequency vectors are parallel to each other with fixed direction in the body-fixed frame. In fact, these two vector have a definite relationship in the wobbling motion, which is nothing other than what is determined by the three moments of inertia (generally the moment-of-inertia tensor [58]). Moreover, when quantized spectra are considered, the tilted-axis cranking gives a description for an isolated band just like the usual cranking does, but the wobbling motion as a whole corresponds to a multiple-band structure, although we have concentrated mainly on the first excited band in this paper.

Although we restricted ourselves to the small amplitude approximation, it is apparently desirable to extend the analysis beyond the RPA; for instance, a detailed comparison of the results with the tilted-axis cranking is only possible in such an analysis. Moreover, as is mentioned in Section 5, the nuclei in which the wobbling

motion is predicted are γ-soft in many cases, so that not only the angular-momentum degrees of freedom but also the shape degrees should be treated without the restriction of the small-amplitude ansatz. This is an important future problem.

Some examples of the realistic calculations are also presented in this paper. The sign relation mentioned above leads us to characteristic types of zigzag behaviour in the E2 and M1 transition probabilities as functions of the rotational frequency, depending on equilibrium values of γ deformation in the (ϵ_2, γ)-plane. This is quite analogous to the case of the B(M1) between the signature-partner bands in odd-A nuclei. An important merit of the microscopic RPA formalism is that the three moments of inertia can be easily calculated, which is highly non-trivial. Their behaviour in three sectors of the (ϵ_2,γ)-plane has been calculated in a rather simplified manner neglecting the self-consistency of the mean-field potential. The results clearly show that their γ-dependence is neither irrotational nor rigid-body-like.

As candidates of the nuclear wobbling motion which might be identified experimentally, we have also investigated the high-spin continuations of the so-called γ-vibrational bands with odd spin in ^{182}Os, ^{124}Xe and ^{126}Ba. The self-consistent triaxiality deformation is somewhat different in each nucleus, and therefore the characteristic features of the collective vibrational modes are shown to be different. Properties of the second-lowest RPA eigenmode, which is in some cases rather collective but does not satisfy the criterion of the wobbling motion, are also discussed.

Throughout this paper the M1 transition between the wobbling and yrast bands has also been kept in scope. It should, however, be noticed that the expressions of the B(M1) in the rotor model are not justified from the microscopic viewpoint. This is because the individual property of quasiparticle orbits is essential for understanding the M1 transitions, which is not taken into account in the macroscopic model, in contrast to the case of the E2 transitions, where the geometrical shape of the nucleus as a whole is mainly responsible. Although the M1 transitions from the quadrupole vibrational band are generally expected to be small at low spin, it has been shown that this is not always the case at the higher-spin region, where the rotation-aligned quasiparticles are present in the vacuum. Note that the M1 transition is only possible if there exists the rotationally induced K-mixing in the RPA phonon amplitudes. As a conspicuous example the high-spin continuation of the odd-spin γ-vibrational band in ^{126}Ba is predicted to have a much stronger M1 transition probability than the $\Delta I = \pm 1$ E2, which is consistent with the observed branching ratio. This strong M1 transition, on the other hand, gives a possible reason for why the $\Delta I = -2$ transition that links the states above and below the band crossing in the odd-spin γ-band has not been observed.

It is worthwhile to stress the importance of the collective-vibrational motions of either the wobbling-like or the γ-vibrational character for understanding the electromagnetic property of the odd-A nuclei. The characteristic property of the vibrational modes reflects strongly on the transition rates through the particle–vibration coupling effects, and therefore the study of the odd-A nuclei gives a valuable testing ground to clarify the character change of the vibrational mode predicted in the present work. We hope that the new generation of large γ-ray detector arrays will provide us with more detailed

information on the electromagnetic transitions, which is necessary to confirm the predictions and to identify the nuclear wobbling motion.

Acknowledgements

Discussions with Daniel Bes and Ramon Wyss are greatly acknowledged. The early stage of this work has been done as a part of the research project on Nonlinear Dynamics of Nuclear Collective Motions, which was organized at the Yukawa Institute, Kyoto, in 1988–1992. We had stimulating discussions with all the members. The computer calculations for this work are financially supported in part by the Grant-in-Aid for Scientific Research from the Ministry of Education, Science and Culture (No. 06234208), and in part by the Research Center for Nuclear Physics, Osaka University. The authors thank Kenjiro Takada for a careful reading of the manuscript.

References

[1] Å. Bohr and B.R. Mottelson, Nuclear deformations, Nuclear structure, Vol. 2 (Benjamin, New York, 1975) ch. 4, p. 190 ff.
[2] E.R. Marshalek, Nucl. Phys. A 331 (1979) 429.
[3] D.R. Bes and J. Kurchan, The treatment of collective coordinates in many-body systems, World Scientific lecture notes in physics, Vol. 34 (World Scientific, Singapore, 1990).
[4] A.K. Kerman and N. Onishi, Nucl. Phys. A 361 (1981) 179.
[5] N. Onishi, Nucl. Phys. A 456 (1986) 390.
[6] K. Kaneko, Phys. Rev. C 45 (1992) 2754; C 49 (1994) 3014.
[7] I.N. Mikhailov and D. Janssen, Phys. Lett. B 72 (1978) 303.
[8] D. Janssen and I.N. Mikhailov, Nucl. Phys. A 318 (1979) 390.
[9] V.G. Zelevinsky, Nucl. Phys. A 344 (1980) 109.
[10] H. Reinhardt, Nucl. Phys. A 381 (1982) 217.
[11] P. Arve, Phys. Lett. B 197 (1987) 307.
[12] J. Kurchan, D.R. Bes and S. Cruz Barrios, Nucl. Phys. A 509 (1990) 306.
[13] J.P. Garrahan and D.R. Bes, Nucl. Phys. A 573 (1994) 448.
[14] Y.R. Shimizu, T. Kisaka and M. Matsuzaki, Soryushiron Kenkyu (Kyoto) 81 No. 6 (1990) F182.
[15] Y.R. Shimizu and M. Matsuzaki, Proc. Int. Conf. on Nuclear structure at high angular momentum, May 1992, Ottawa, AECL-10613, pp. 278–282.
[16] Y.R. Shimizu and M. Matsuzaki, Proc. Int. Conf. on Physics from large gamma-ray detector arrays, August 1994, Berkeley, CA, LBL-35687, pp. 40–44.
[17] E.R. Marshalek, Phys. Rev. C 11 (1975) 1426; Nucl. Phys. A 266 (1976) 317.
[18] J.L. Egido, H.J. Mang and P. Ring, Nucl. Phys. A 339 (1980) 390.
[19] Y.R. Shimizu and K. Matsuyanagi, Prog. Theor. Phys. 70 (1983) 144; 72 (1984) 799.
[20] M. Matsuzaki, Y.R. Shimizu and K. Matsuyanagi, Prog. Theor. Phys. 79 (1988) 836.
[21] F. Dönau, Nucl. Phys. A 471 (1987) 469.
[22] Å. Bohr and B.R. Mottelson, Nuclear deformations, Nuclear structure, Vol. 2 (Benjamin, New York, 1975) ch. 4, p. 158 ff.
[23] M. Baranger and K. Kumar, Nucl. Phys. A 110 (1968) 490.
[24] H. Sakamoto, Nucl. Phys. A 557 (1992) 583c.
[25] K.E.G. Löbner, M. Vetter and V. Hönig, Nucl. Data Tables A 7 (1970) 495.
[26] L.D. Landau and E.M. Lifshitz, Mechanics, Course of theoretical physics, Vol. 1 3rd Ed. (Pergamon, London, 1976) ch. 37.

[27] M.M. Villard, Ph. Hubert and R.J. Liotta, Phys. Scripta 26 (1982) 201.
[28] M. Matsuzaki, Nucl. Phys. A 509 (1990) 269.
[29] C.G. Andersson et al., Nucl. Phys. A 361 (1981) 147.
[30] J. Skalski, Nucl. Phys. A 473 (1987) 40.
[31] H. Kurasawa, Prog. Theor. Phys. 64 (1980) 2055; 66 (1981) 1317; 68 (1982) 1594.
[32] D.R. Bes, private communication.
[33] Y.R. Shimizu, J.D. Garrett, R.A. Broglia, M. Gallardo and E. Vigezzi, Rev. Mod. Phys. 61 (1989) 131.
[34] P. Ring and P. Schuck, The nuclear many-body problem (Springer, Berlin, 1980).
[35] G.B. Hagemann and I. Hamamoto, Phys. Rev. C 40 (1989) 2862.
[36] D. Cline, Annu. Rev. Nucl. Part. Sci. 36 (1986) 683.
[37] P. Chowdhury et al., Nucl. Phys. A 485 (1988) 136.
[38] W. Gast et al., Z. Phys. A 318 (1984) 123.
[39] G. Puddu, O. Scholten and T. Otsuka, Nucl. Phys. A 348 (1980) 109.
[40] S. Törmänen et al., Nucl. Phys. A 572 (1994) 417.
[41] R. Wyss et al., Nucl. Phys. A 505 (1989) 337.
[42] Å. Bohr and B.R. Mottelson, Single-particle motion, Nuclear structure, Vol. 1 (Benjamin, New York, 1969) ch. 3-3b.
[43] D. Ward et al., Nucl. Phys. A 529 (1991) 315.
[44] D.C. Radford et al., Nucl. Phys. A 545 (1992) 665.
[45] M. Oshima et al., Phys. Rev. C 37 (1988) 2578.
[46] I. Hamamoto and B.R. Mottelson, Phys. Lett. B 132 (1983) 7.
[47] A. Ikeda, Nucl. Phys. A 439 (1985) 317.
[48] N. Onishi, I. Hamamoto, S. Åberg and A. Ikeda, Nucl. Phys. A 452 (1986) 71.
[49] M. Matsuzaki, Nucl. Phys. A 491 (1989) 433; A 519 (1990) 548.
[50] R. Bengtsson et al., Nucl. Phys. A 415 (1985) 189.
[51] I. Hamamoto and B. Mottelson, Phys. Lett. B 127 (1983) 281.
[52] A. Ikeda and S. Åberg, Nucl. Phys. A 480 (1988) 85.
[53] N. Onishi and N. Tajima, Prog. Theor. Phys. 80 (1988) 130.
[54] M. Matsuzaki, Nucl. Phys. A 504 (1989) 456.
[55] C.-H. Yu et al., Nucl. Phys. A 511 (1990) 157.
[56] M. Matsuzaki, Phys. Rev. C 46 (1992) 1548.
[57] S. Frauendorf, Nucl. Phys. A 557 (1993) 259c.
[58] A.L. Goodman, Phys. Rev. C 45 (1992) 1649.
[59] R.G. Helmer, Nucl. Data Sheets 64 (1991) 79.
[60] H. Kusakari et al., JAERI Tandem annual report (1992) p. 125.
[61] R.M. Ronningen et al., Phys. Rev. C 26 (1982) 97.
[62] B. Kotliński et al., Nucl. Phys. A 517 (1990) 365.